



Master thesis

Lars Dalskov Mosgaard

Propagation of Sound in Lipid Membranes

Academic advisor: Thomas Heimburg

Secondary advisor: Andrew Jackson

Submitted: 03/11/2011

Use the right level of description to catch the phenomena of interest. Don't model bulldozers with quarks.

-Nigel Goldenfeld and Leo P. Kadanoff

Acknowledgments

First of all I want to thank my lead supervisor Thomas Heimburg and my secondary supervisor Andrew Jackson. You have been a continuous sources of inspiration and support – thank you. I would like to thank Jayanta Bhattacharjee for his invaluable help in understanding his and his coauthors brilliant work in the field of ultrasonic attenuation in critical mediums. Further, thanks to William W. Van Osdol for providing the means to compare his and his coauthors work with the here found analytical expression for the dynamic heat capacity.

I would also like to thank all the wonderful people that have help me with proofreading: Vedran Sekara, Stanislav Landa, Pradeep Ramesh and Silja Heilmann. I would like to thank the complete BioComplexity group for wonderful company and a big thanks to the KC1 crew for helping me through the process of writing this thesis, both academically and emotionally. Finally, thanks to my family that in all aspects of my education have been an infinite source of support – thank you.

Note on programs

All simulations have been written in **FORTRAN**. Multiple versions of Intel's fortran compiler (**ifort**) have been used for compilation, though all newer then 2008. Data treatment have been carried out along with plotting and fitting in **MATLAB R2010b**. Image handling has been done in **Inkscape**. Additionally, **Wolfram Mathematica 8** has been used for mathematical support.

Resumé

Med introduktionen af Soliton-modellen er forståelse af lydudbredelse i lipidmembraner blevet vital for forståelsen af hvordan nerver sender signaler langs deres axoner. Målet med dette speciale er at bygge en forståelse for hvordan lavfrekvent lydudbredelse i lipidmembraner, og hermed hvordan denne lydudbredelse afhænger af frekvens. Min indgangsvinkel er af termodynamisk nature og dækker over både analytisk og numerisk arbejde. Det numeriske arbejde dækker udforsking af lipidmembraners relaksationsegenskaber og en undersøgelse af hvordan lipidfaseovergangen påvirkes af et varme reservoir af endeligt størrelse. Med det sidst nævnte numeriske arbejde er det muligt at koble lipidmembraners reaktion på lyd til lydhastigheden og hermed muliggøre en detaljeret forståelse af lyd udbredelse i lipidmembraner. Jeg finder, at lydudbredelse i lipidmembraner er kraftigt afhængig af frekvens, også ved meget lave frekvenser, og ligeledes er kraftigt afhængig af densitet.

Abstract

With the emergence of the Soliton model, understanding low frequency sound propagation in lipid membranes has become essential for understanding how nerve signals propagate. My thermodynamic approach employs both analytic arguments regarding sound propagation as well as numerical explorations of membrane relaxation behavior, and how the lipid melting transition is affected by a finite heat reservoir. Based on the last mentioned numerical work, a connection between the response of the lipid membrane to sound and the speed of sound is made, enabling me to estimate the frequency dependence of sound in lipid membranes for low frequencies. I find dispersion, even at very low frequencies, to be very strong and to strongly depend on lateral density.

Contents

1	Introduction	1
2	Background Theory	5
2.1	Lipid Membranes	5
2.1.1	Introduction to Lipids	7
2.1.2	Membrane Phases	8
2.1.3	Membrane Phase Transition	9
2.2	Theory of Nerve Signals	13
2.2.1	H & H Model	14
2.2.2	Soliton Model	17
2.3	Sound	21
2.3.1	Introduction to Sound	21
2.3.2	Distortion of Sound	23
2.3.3	Sound Propagation near Phase Transitions	24
3	Analytic Approach	27
3.1	Adiabatic Perturbations	28
3.2	Compressibility	32
3.3	Speed of Sound	35
3.4	Dispersion	38
4	Simulations	41
4.1	Modeling	41
4.1.1	Doniach Model	41
4.1.2	Monte Carlo Method	44
4.1.3	Implementation	46
4.1.4	Simulation of the Doniach Model	47
4.2	Relaxation Simulations	49
4.2.1	Fluctuation Simulations	50
4.2.2	Perturbation Simulations	52
4.3	Finite System Simulations	59
4.3.1	Adiabatic Model Extension	59
4.3.2	Results	65

5 Discussion and Conclusion	69
5.1 Discussion	69
5.2 Conclusion and Perspectives	72
Bibliography	75
A Thermodynamics	II
A.1 Susceptibilities	II
A.2 Relaxation Time	IV
B Equation of Sound	VI
B.1 Fluid Dynamics	VII
C Derivations	IX
C.1 Latent Heat of Expansion	IX
C.2 Phase velocity	X
D Linear Response Theory	XII
E Simulations	XIV
E.1 Detailed Balance of the Adiabatic Model	XIV
E.2 Equilibration	XV
E.3 Finite Size Effects	XVI
E.4 Calculation of Errors	XVI
E.4.1 The Blocking Method	XVII
E.4.2 The Jackknife Method	XVIII
E.5 Adoptive Algorithm	XVIII

Chapter 1

Introduction

Biological membranes are ubiquitous in the living world. Despite their diversity, membranes are remarkably similar in structure and composition, and exhibit similar thermodynamic properties. They exist as thin, almost two-dimensional lipid bilayers whose primary function is to separate the interior of cells and organelles (sub-cellular compartment) from their external environments. This separation in turn leads to the creation of chemical and biological gradients, which play a pivotal role in many cellular and sub-cellular processes, e.g. Adenosine Tri-Phosphate (ATP) production. Given the importance of such chemical gradients across membranes, it is unsurprising that cells have invested heavily in infrastructure pertaining to inter- and intra-membrane signaling and transport.

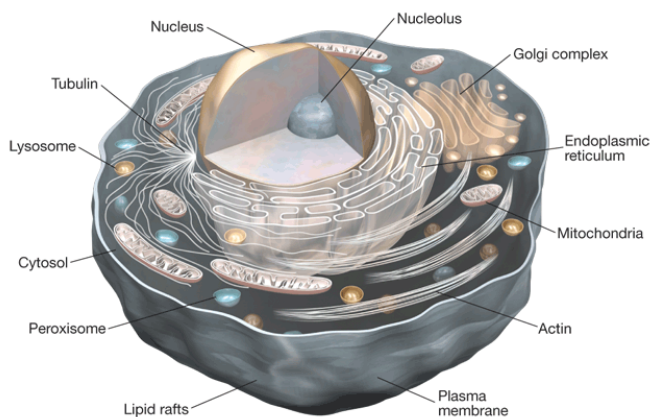


Figure 1.1: A idealized illustration of an animal cell, showing the outer membrane and the inner organelles. From [1].

Even the propagation of nerve signals which allows cells to communicate quickly over long distances has been attributed to biological membranes, specifically the membrane of nerves, an ability that is vital for higher life-

forms as animals [2,3].

In 1952, Hodgkin and Huxley [2] proposed the now commonly accepted theory for propagation of nerve signals. Their model is based on the equilibration of a trans-membrane ionic gradient through specific ion-conducting proteins (ion-channels), resulting in a transient voltage change over the membrane. This voltage change causes an avalanche phenomena by which the nerve signal propagates down the axon. Hodgkin and Huxleys' theory can be schematically represented as a sequence of Kirchhoff circuits, where the membrane acts as a capacitor and the ion-channels function as resistors. In this representation, neuronal propagation is modeled as being dissipative in nature – meaning that the process generates heat. Experimental measurements of signal propagation in neurons do however not show a net generation of heat, suggesting, contrary to Hodgkin and Huxleys' predictions, that the process is adiabatic [4–7].

To resolve this contradiction, Heimburg and Jackson [3] have recently proposed a model where nerve signals are treated as a propagation of localized density pulses (solitons) in the nerve axon membrane. The foundation of the Soliton model is the adiabatic nature of the propagation of nerve signals. With this alternative model the Heimburg and Jackson are able to make correct predictions regarding the propagation velocity of the nerve signal in myelinated nerves, along with a number of new predictions regarding excitation of nerves and the role of general anesthetics [8]. In addition, the Soliton model explains a number of observations about nerve signal propagation, which are not included in the Hodgkin and Huxley model, such as changes in the thickness of the membrane, changes in the length of the nerve and the existence of phase transition phenomena [9].

Biological membranes exhibit a phase-transition between an ordered and a disordered lipid phase near physiological conditions [10]. It has also been shown, that organisms alter their detailed lipid composition in order to preserve this phase-transition despite different growth conditions [11–13]. Near a phase transition the behavior of the membrane changes quite drastically: The thermodynamic susceptibilities, such as heat capacity, display spikes and the characteristic relaxation times of the membrane show a drastic slow down [14–18]. The biological implications of membrane phase-transitions continues to be an area of active research.

As previously noted, the existence of a phase transition in a membrane drastically affects, among other, its compressibility, which in turn affects how sound propagation in a membrane, see Fig. (1.2).

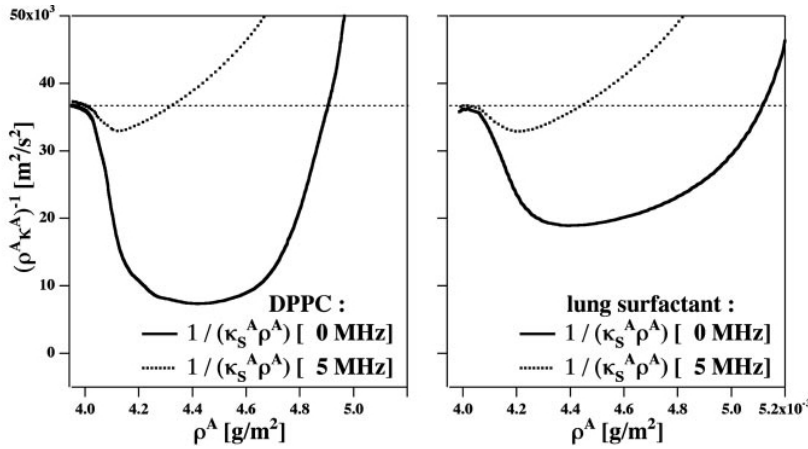


Figure 1.2: The speed of lateral sound at the theoretical low frequency limit (0 Hz) and at 5 MHz , from ultra-sonic experiments, as a function of lateral density. *Left*, large unilamellar vesicles of DPPC at $T = 45 \text{ }^\circ\text{C}$. *Right*, lung surfactant at $T = 37 \text{ }^\circ\text{C}$. Figure has been adopted from [3].

Fig. (1.2) clearly suggests that the speed of sound in lipid membranes is a function of frequency (dispersion) and a non-linear function of density. In order for solitons to exist in a given medium, the speed of sound in the medium necessarily has to have a non-linear relationship with the density, an effect which again has to be countered by dispersion. It is exactly the cancellation of the non-linear and dispersion effects that causes the soliton. These criteria are met in artificial lipid membranes as well in naturally occurring membranes entirely due to the presence of the phase transition. It is these observations that allow Heimburg and Jackson [3] to predict the presence of solitons in lipid membranes.

With the introduction of the Soliton model [3], understanding sound propagation in lipid membranes has become important for understanding nerve signals. From the duration of nerve signals (milliseconds) the relevant frequency regime for nerve signals can be estimated to be below 1000 Hz . The details of the dispersion in this regime is however not known. The few experimental efforts in this low frequency regime have been aimed at exploring the relaxation behavior of the lipid membrane [17, 18]. In the present form of the Soliton model, the dispersion effects have been assumed to be small and independent of density, and the assumed values for the dispersion are estimated from the physical length of nerve pulses. These approximation have been necessary due to the lack of data regarding the dispersion at low frequencies in lipid membranes.

Beyond this apparent use, the dispersion of sound in a medium is strongly related to the dynamical properties of the membrane in general, and there-

fore holds significant importances for the understanding the properties of lipid membranes. An example of this, is the intimate relationship between sound propagation and a medium's viscosity.

The main goal of this thesis is to explore the dispersion effects of sound propagation in lipid membranes at low frequencies and through these studies to create a toolbox to understand this process from a thermodynamical point of view.

The thesis is structured as following: Starting out the reader will be introduced to the **Background Theory** (chapter 2), containing an introduction of the lipid membrane, nerve theory and theory of sound. This lead to the **Analytical Approach** (chapter 3), where the frequency dependence of the lateral speed of sound in lipid membranes is estimated analytically, based on thermodynamics and linear response theory. The analytical efforts are backed by simulations (Monte Carlo) and modeling, directly or conceptually, in the following chapter on **Simulations** (chapter 4). Ending with the discussion of the findings and the process leading to these in **Discussion and Conclusion** (chapter 5).

Chapter 2

Background Theory

In the following chapter the relevant theory and concepts will be introduced. Starting out, the medium of interest (the lipid membrane) will be introduced along with insight into nerves and how nerve signals are believed to be conducted. Ending with a general introduction to sound.

2.1 Lipid Membranes

Overton [19] proposed in 1899 that cells are surrounded by a “fatty oil”. In 1925 Gorter and Grendel [20] extended this, by finding that cells “are covered by a layer of fatty substances that is two molecules thick”. Further, it became clear in 1935 from experiments made by Danielli and Harvey [21] that the fatty layer is made up of both lipids and proteins. These discoveries lead to years of speculation about the organization of these fatty layers. In 1972 Singer and Nicolson [22] proposed the *Fluid Mosaic model*. The Fluid Mosaic model describes the structure of the fatty layer as a homogeneous bilayer of lipids (“a two-dimensional oriented viscous solution” [22]), wherein proteins and other macro-molecules can be anchored or immersed due to mainly hydrophobic interactions, see Fig. (2.1), *left*, for visualization. The idea of the Fluid Mosaic model was extended in 1984 by Mouritsen and Bloom [23] in the *Mattress model*. In the Mattress model the bilayer is viewed as a pseudo 2-dimensional heterogeneous solution, where mismatching between the hydrophobic regions of the lipids and the proteins induce inhomogeneities in the bilayer, see Fig. (2.1), *right*.

Both models describes the membrane as a dynamic structure. Already before the introduction of the Mattress model it became evident that the mechanical and fluid dynamical properties of natural occurring membranes are crucial for the cells and biology [17]. In the efforts of understanding these properties, it became apparent that membranes can be found in a number of smectic phases and that the phase transitions between these often are close

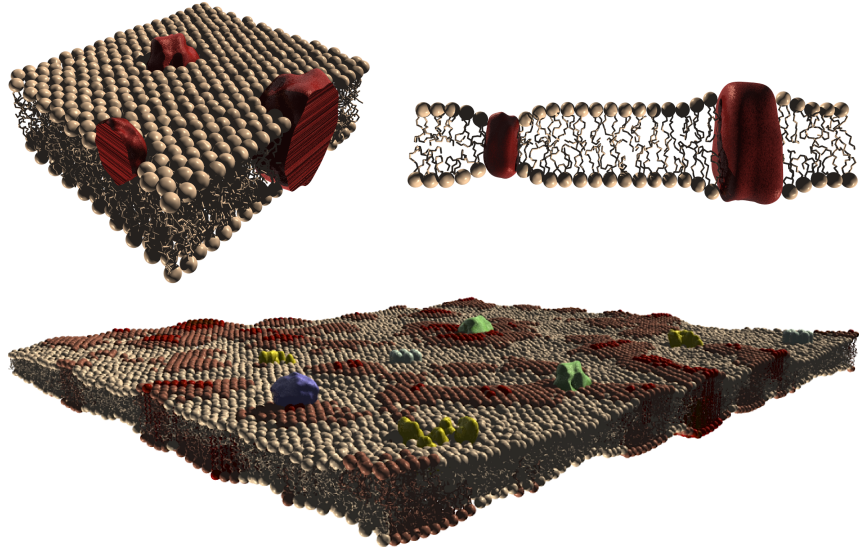


Figure 2.1: Patches of membrane in accordance with; *left*, the Fluid Mosaic model, *right*, the Mattress model. *Bottom*, modern view of the membrane, where the membrane is considered to be a highly heterogeneous and dynamic structure. The illustration has been provided by Andreas Blicher.

to physiological conditions. These phases, the transitions and their mechanical and dynamical implications for the physical properties of membranes have been the focus of both intense experimental and theoretical studies.

The lipid composition of biological membranes varies, different types of tissue can have very different compositions – also growth criteria can alter the composition. It has been shown that *E. coli* grown at different temperatures alter their lipid composition such that their membranes show similar physical properties at their respective growth conditions [11]. Similar lipid composition changes have also been observed for trouts. Specifically, changes in lipid composition of liver tissue of trouts raised at different temperatures [12]. It has further been observed that lipid composition changes take place in deep-sea bacteria grown at different pressure [13]. All these experimental findings indicate that the physical properties of biological membranes are tightly controlled, further underlining the importance of these properties for the functionality of the membrane and therefore biology.

Before exploring membrane properties and their different phases further, an introduction to lipids is necessary.

2.1.1 Introduction to Lipids

A variety of lipids is found in biological membranes, these can be divided up into sterols (e.g. cholesterol), sphingolipids and phospholipids. In cell membranes the majority of lipids are phospholipids, these have, as the majority of all lipids in membranes, a polar and non-polar region making them amphiphilic molecules.

The non-polar region is in phospholipids composed of two hydrocarbon chains typically containing 16 or 18 carbons molecules [24]. The length can though vary from 12 to 22 molecules and the chain can be either saturated, unsaturated (containing double bonds) or one of each which is the most common. The hydrocarbon chains are linked through ester bonds to adjacent carbons of a glycerol backbone. The last carbon in the glycerol backbone is, in the case of a phospholipid, linked to a negativity charged phosphate group via another ester bond. To this phosphate group the head group is attached, making up the polar region of the lipids. The head group can be a number of different biological compounds such as choline, ethanolamine, serine and glycerol. Both serine and glycerol head groups will result in a net negative charge of the polar region, whereas with choline and ethanolamine the region will be zwitterionic¹, all at neutral pH. In the majority of biological membranes about 10 – 20% of the lipids are charged, up to 40% can be found in the membranes of mitochondria [25].

The naming convention for phospholipids is based on the lipid chains and on the head group. For example, two palmitic acids linked to a choline group is called dipalmitoylphosphatidylcholine (DPPC). DPPC is depicted in Fig. (2.2) (a).

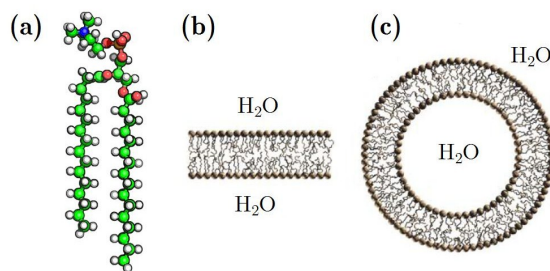


Figure 2.2: (a): Illustration of a 1,2-dipalmitoylphosphatidylcholine (DPPC) lipid. (b): A patch of a bilayer. (c): Unilamellar vesicle. The illustration has been provided by Andreas Blicher

Due to the amphiphilic nature of the majority of lipids, they will when mixed with a polar solvent (e.g. water) self-organize to minimize unfavor-

¹Zwitterionic means no net charge but the charges are separated making it very polar.

able polar-nonpolar interactions. This self-organization will result in the formation of macroscopic structures, such as micelles, planar bilayers (see Fig. (2.2) (b)) or vesicles (see Fig. (2.2) (c)). In general other non-lamellar structures can be formed, but they are rarely observed in excess water. Especially vesicles is of general interest in the context of biological membranes. These bilayer structures are energetically favorable and are identical in structure to native biological membranes - thus representing a valuable model system for studying physical properties of biological membranes. Throughout this thesis large unilamellar vesicles of DPPC will be used as a model system for biological membranes.

2.1.2 Membrane Phases

Lipid bilayers can be found in a number of smectic phases² vary with lipid composition. Common for these phases is that they are neither crystalline nor fluid, they share properties from both classes.

Lipid bilayers are considered to have four smectic phases. The customarily designated procedure for the lipid bilayer phase is following: For describing the long-range ordering an upper-case letter is used; L one-dimensional lamellar, and P for two-dimensional oblique. A lower-case subscript is used to describe the short-range ordering of the lipid chains; α disordered (fluid); β , ordered - not tilted with respect to the normal of the bilayer (gel); β' , ordered, tilted (gel) [26]. The four phases are presented below in the generalized sequence of thermotropic transitions [27]:

- L_c : Crystalline phase, in which the lipids are ordered in three dimensions.
- L'_β : Crystalline molecular order. Chains are mostly “all-trans”³ ordered and tilted. Lipids are in this phase packed in a distorted quasihexagonal lattice. This phase is often called the solid phase or simply the gel phase.
- P'_β : So called “ripple” phase. The membrane is partially solid, partially fluid organized in a periodic structure in the plane of the lamellae. The lipid chains are tilted but packed in a regular hexagonal lattice. This phase forms prior to chain melting.
- L_α : Lipid chains are disordered. Order of lattice is lost. This phase is often called the liquid-disordered phase or simply the fluid phase.

The main interest in this thesis is the main lipid melting transition between L'_β and L_α , where the ripple phase will be ignored. The ripple phase has been

²By a phase is meant a state of a medium that share physical properties.

³Spatial orientation of the two chains.

shown to be easily abolished by the presence of various biomolecules in the membrane, and is rarely seen in biological membranes [28]. The topology of the gel and fluid phases is illustrated in Fig. (4.7).

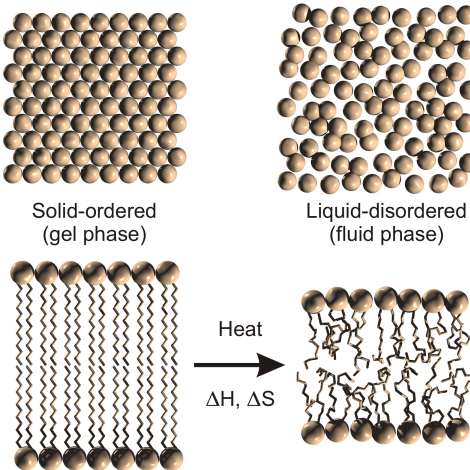


Figure 2.3: *Top*, illustrates the lateral ordering of the gel phase (*left*) and the fluid phase (*right*). The *bottom* depicts the ordering of the lipid chains. The illustration is provided by Andreas Blicher

2.1.3 Membrane Phase Transition

A *phase transition* is defined as a transformation from one phase of a system to another, e.g. ice to water. Depending on the nature of the transition, a system undergoing a phase transition can display a number of extraordinary properties, such as drastic changes in the susceptibilities and in the relaxation behavior of the system.

The lipid melting transition has been found take place just under the physiological growth temperature in naturally occurring membranes, see Fig. (2.4). As previously mentioned, organisms have been found to adapt their lipid composition such that their membranes conserve their physical properties at different growth condition, this includes the lipid melting transition. Organisms shift their membranes lipid melting transition such as to conserve the relation between the transition and their growth conditions, even under extreme conditions [11]. The close relation between that lipid melting transition and growth conditions indicates the importance of the transition for the function of biological membranes and therefore biology in general. This has motivated extensive research of the nature of the main lipid melting transition between the gel- and fluid-phase [26, 29, 30].

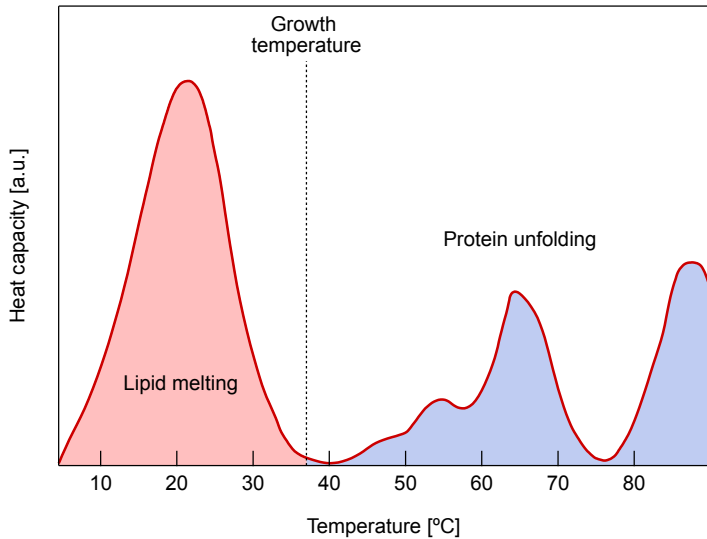


Figure 2.4: The calorimetric profile of an intact *E. coli* membrane. The red shaded region is associated to the lipid transition, whereas the blue region is associated to protein unfolding. Notice that the lipid transition is immediately below the growth temperature. The figure is adopted from [11].

The lipid melting transition⁴ is an exothermic transition occurring over a narrow but finite temperature range, which is driven by the entropy gain of collective melting of lipid chains. The exothermic transition is easily monitored by differential scanning calorimetry (DSC), where the heat capacity show a spike during the transition of finite extent. The transition associated heat capacity is referred to as the excess heat capacity. During the transition a number of other susceptibilities likewise display spikes, of major importance for this thesis is the compressibility and lateral compressibility.

The thermodynamics of the lipid melting transition can be described by considering the lipids as being in only two distinct states, gel- and fluid state. This however does not imply that the membrane is well described by only two distinct states. During the transition, the membrane can be found in a number of intermediate states where the two lipid states are mixed. The mixing of the two states is a result of the cooperativity of the transition being finite. The extent of the cooperativity in the transition is reflected in the width of the transition, which varies from more than 30 K for naturally occurring membrane to around 0.1 K for multilamellar vesicles. In both cases the lipid melting transition should though be considered as a highly cooperative process.

⁴In the literature the main lipid phase transition is classified as a weak first order transition, which is close to the critical point where the transition becomes second-order [17, 29].

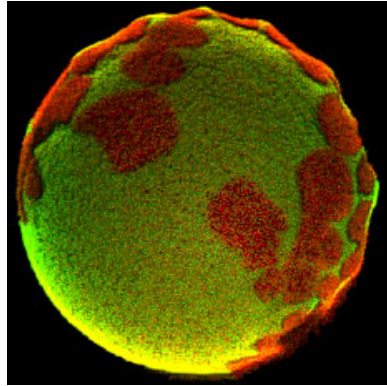


Figure 2.5: Fluorescence image of a lipid vesicle. The coloring indicates domains of lipids in the gel state (*red*) and in the fluid state (*green*). The image is from [31].

The topography of the membrane during the lipid melting transition is dominated by the formation of domains of various sizes and compositions (see Fig. (2.5)), though phase separation is not observed⁵. The domains are stabilized by the interplay between configuration entropy and interfacial associated free energy. The fluctuations of these cooperative domains display very slow relaxation times in the transition region [32]. The extent of this slow down during the lipid melting transition result in the characteristic relaxation time to be in the second regime for pure lipid membranes [18].

The transition temperature is defined as the temperature where both lipid states (gel- and fluid state) are equally probable

$$\frac{p_{fluid}(T_m)}{p_{gel}(T_m)} = \exp\left(-\frac{\Delta G}{RT_m}\right) = 1 \Rightarrow \quad (2.1)$$

$$\Delta G = \Delta H - T_m \Delta S = 0 \Leftrightarrow T_m = \frac{\Delta H}{\Delta S}, \quad (2.2)$$

where T_m is the transition temperature, ΔS is the entropy change and the ΔH is the enthalpy change associated with the transition. The change in enthalpy is experimentally readily available from differential scanning calorimetry, where the enthalpy change is the integral of the excess heat capacity. Commonly the peak of the transition is a close approximation to the transition temperature and can in the literature be referred to as such.

From Eq. (2.2), any physical parameter that can alter either ΔH or ΔS will shift the position of the transition. Since most lipids have either a charged or a zwitterionic head group, changes in electrical fields will induce a change

⁵This observation is at odds with a true first order phase transition, which display complete phase separation that renders interface phenomena unimportant.

in the position of the transition. Lipids in the gel- and the fluid states have different in-plane packing and physical sizes (see Fig. (4.7)), resulting in a area increase of about 25% and a volume increase of about 4% [33]. From this, changes in pressure and lateral pressure will also result in a shift of the position of the transition. In general a number of different factors have been found to have strong influence on the transition properties, among these are: Membrane hydration [34], salt concentration (especially of divalent cations) [35], the presence of cholesterol, peptides, neurotransmitters, antibiotics and general anesthetics (e.g. alcohol, chloroform etc.) [36, 37]. High bending curvature of the membrane and vesicle size can also affect the lipid melting transition [38]. These “handles” on the lipid membrane transition illustrate the diversity and also the generality of the lipid melting transition.

Proportionality Relations

A number of extraordinary relations between thermodynamical variables of the lipid membranes system have been found to hold in the transition range. Ebel *et al.* [33] showed through extensive experimental work, that the change in system enthalpy is proportional to the change in volume,

$$\Delta V = \gamma_V \cdot \Delta H, \quad (2.3)$$

where the proportionality constant for large unilamellar vesicles (LUV) of DPPC is $\gamma_V = 8.599 \cdot 10^{-10} \text{ m}^3/\text{J}$ [39]. This relation holds for artificial lipid membranes as well as for natural occurring membranes [33]. Recently it have been shown by Molecular Dynamics (MD) simulations that this proportionality relation is valid in general, not just in the transition region [40].

Based on the cooperative nature of this proportionality relation, Heimburg [39] proposed that a similar proportionality relation should hold between change in enthalpy and change of area. The relation has been justified indirectly by lipid monolayer experiments [41].

$$\Delta A = \gamma_A \cdot \Delta H, \quad (2.4)$$

where the proportionality constant for LUV of DPPC is $\gamma_A = 8.93 \cdot 10^{-1} \text{ m}^2/\text{J}$ [39]. This relation is of great interest for this thesis since it posses a direct link between the easily measurable excess heat capacity, Δc_P , and the transition associated part of the isothermal lateral compressibility, $\Delta \kappa_T^A$.

$$\Delta \kappa_T^A = \frac{\gamma_A^2 T}{\langle A \rangle} \Delta c_P \quad (2.5)$$

See Appendix: **Susceptibilities** (appendix A.1) for details of derivations.

2.2 Theory of Nerve Signals

In this section, the textbook theory for conduction of nerve signals will be introduced, and discussed in the context of experimental findings that contradict this theory. These contradictions have lead to the proposal of a alternative theory which also will be introduced.

Already in the ancient Greece, Galen of Pergamon philosophized over the human (or animal) ability to control its limbs, to feel pain etc. He deducted that the head is the controlling unit of the body. As soon as this realization was made, the next question was how the head is able to communicate with the rest of the body [42]. It was found that signaling is conducted through a cell-type called nerves or neurons. The “typical” nerve attributed long distance communication (e.g. brain to leg) can be schematically depicted as shown in Fig. (2.6)

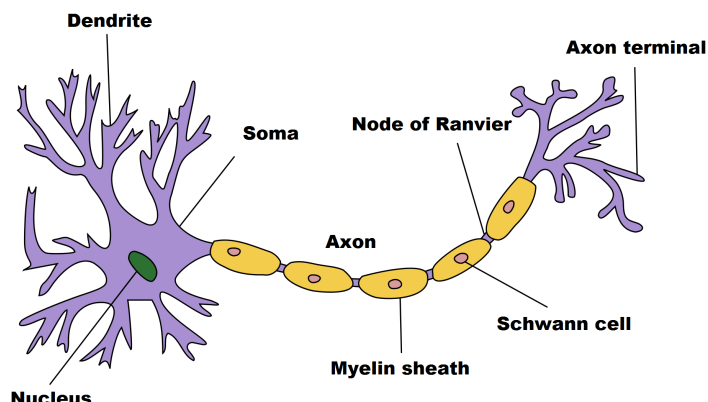


Figure 2.6: A schematic illustration of a nerve. Nerve cells are in principal not that different from other cells, having a nucleus, a cell membrane, mitochondria etc. Unique to nerves are dendrites, axon and axon terminals. Dendrites are attributed a sensory role, where a nerve signal is started. The axon are attributed conduction of the nerve signal through the length of the nerve – possibly over meters. In the axon terminals the nerve signal is transmitted onto other tissue. The Illustration have been adopted from [Wikipedia – Neuron](#).

When considering the propagation of nerve signals (also refereed to as nerve pulses) the main point of interest is the axon. The length of a nerve axon can span from nanometers to meters. Geometrically the axon can be forked, but a single cylindric geometry is commonly assumed for simplification. There can be a number of support tissues surrounding the axon – of special interest is the myelin sheaths or layers, they are formed by Schwann that are cells wrapped around the nerve axon. Myelinated nerves have been found to transmit signals much faster ($\sim 100 \text{ m/s}$) then non-myelinated nerves ($\sim 1 - 5 \text{ m/s}$) [11]. From the propagation velocities and the duration

of the nerve pulses, the physical length of a nerve pulse can be calculated to be in the range from millimeters to centimeters, marking nerve pulses as macroscopic phenomena.

2.2.1 Hodgkin & Huxley Model

In 1791 Luigi Galvani discovered that he could get the legs of dead frogs to move by stimulating the spine electrically. With this finding, the road was paved for describing nerve signaling as being of electrical nature. In 1952 Hodgkin and Huxley [2] presented a mathematical model for the initiation and propagation of nerve pulses in giant squid axons. Their effort was originally only intended as an empirical description of the experimentally found transient voltage change of a nerve signal (or action potential) by Cole and Curtis [43]. Their description however gained widespread acceptance throughout the neural field, resulting in them receiving the Nobel prize in medicine in 1963.

The giant squid axon was early on found to have a significantly high potassium concentration inside the nerve compared to outside and a higher sodium concentration outside than inside. These concentration differences give rise to a voltage difference (through the Nernst potential) over the nerve membrane. Hodgkin and Huxley [2] assumed that the cell membrane acts like a barrier, in which trans-membrane ion channels are embedded. These ion channels are assumed to be voltage gated and specific in their conduction of ions – either conducting sodium or potassium. In their view, the membrane is considered impermeable to ions and is assumed to be equivalent in function to a capacitor with constant capacitance. This is schematically depicted in Fig. (2.7) A.

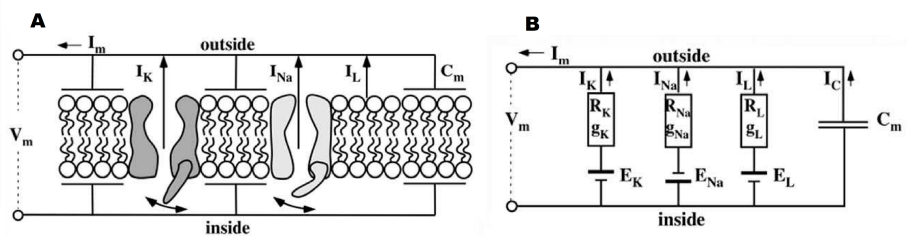


Figure 2.7: A: Illustration of the axon membrane in view of the Hodgkin-Huxley model. B: The equivalent electrical circuit of the membrane, where the ion channels are replaced with resistors and the membrane acts as a capacitor. The figure has been adopted from [11]

Hodgkin and Huxley's basic idea was that a local depolarization will lower the potential difference over the membrane causing a local flux of ions through the channels. This will result in further depolarization of the mem-

brane which in turn will cause additional channels to conduct ions, hereby creating a cascade effect through which the nerve signal is propagated. The beauty of their model is that the axon membrane can be depicted as a rather simple basic electrical circuit unit. The equivalent circuit can be seen in Fig. (2.7) *B*. Though the basic equivalent circuit seem quite straightforward, the detailed dynamics of the ion channels is rather complicated. The ion channels have a complex time and voltage dependence which have to be empirically fitted for any system under consideration.

Hodgkin and Huxley proposed the following differential equation for describing the propagation of the voltage pulse in a nerve (giant squid axon),

$$\frac{a}{2R_i} \frac{\partial^2 U}{\partial x^2} = C_m \frac{\partial U}{\partial t} + g_K(U - E_K) + g_{Na}(U - E_{Na}) + g_l(U - E_l), \quad (2.6)$$

where U is the voltage, which is a function of time and position, R_i is the resistivity along the interior of the nerve, C_m is the capacitance of the membrane and a is the radius of the axon. Here the geometry of the axon has been assumed to be a perfect cylinder. E_K and E_{Na} are the respective *resting* potentials associated to potassium and sodium, with E_l being the leak potential. g_K , g_{Na} are conductance of potassium and sodium respectively, and g_l is the leak conductance, all being complicated functions of voltage and time.

The authors themselves are in their original paper very humble about the generally appliance of their model, being well aware of the empirical nature of it. The empirical aspect of their model makes its application to any new system a tedious job, where many of the parameters can not be measured in experiments directly. Despite the empirical nature of the Hodgkin-Huxley model (HH-model), it is able to reproduce the voltage pulse in the giant squid axon quite nicely with good estimation of the pulse propagation speed.

Discrepancies of the Hodgkin-Huxley Model

The assumptions made by Hodgkin and Huxley imply that the membrane is constant structure with no drastic changes in geometry or any other physical property. These assumption seem in conflict with the dynamic nature of lipid membrane, especially in the vicinity of the lipid melting transition. Experimental findings even indicates the occurrence of a phase transition during the nerve pulse [44, 45]. Furthermore, the very complex and selective gating of the ion channels can in itself be questioned. Tasaki *et al.* [46] showed that the axon of a giant squid can still accommodate propagation of nerve pulses with no monovalent cations in the exterior solution (e.g. Na, K). In the literature this contradicting observation has been attributed to

secondary selectivity of the ion channels, which though seem an unsatisfactory explanation.

In the equivalent circuit terminology, the ion channels are viewed as resistors through which ion (charges) flow. This is a strictly dissipative process independent of flow direction. The HH-model describes the action potential as being produced entirely by ion flows⁶, making the propagation of nerve signals a stringently dissipative process. Hill *et al.* [4] published in 1958 a review on the heat production of a nerve pulse, showing that during a nerve pulse heat is first released and then entirely reabsorbed, following the profile of the electrical pulse within experimental errors. This fundamental finding have later been confirmed in great detail for nerves originating from a number of different myelinated [7] and non-myelinated [5, 6] nerves. The re-absorption of the produced heat strictly classifies the nerve pulse as an adiabatic process (see Fig. (2.8), b), which is very much at odds with the dissipative nature of the HH-model.

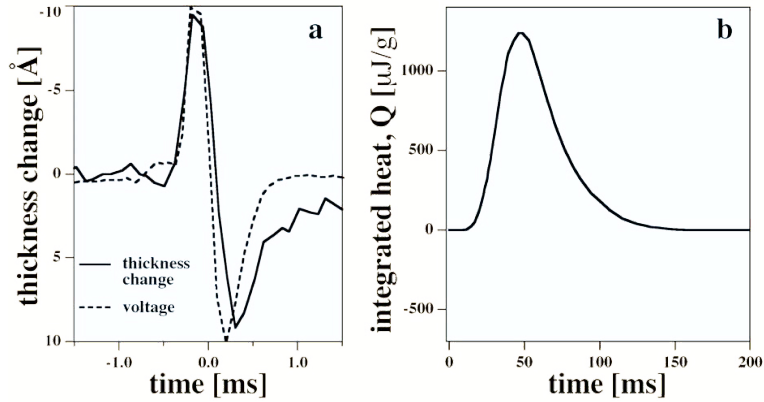


Figure 2.8: During the nerve pulse the thickness and the heat of the nerve axon changes. *a*: Shows that thickness change scales with the electrical nerve pulse. Experiment was conducted on giant squid axons. The figure has been adopted from [47]. *b*: Shows the integral of the heat released during a nerve pulse, showing no net production of heat. Experiments were conducted on non-myelinated fibers of the pike olfactory nerve. The figure has been adopted from [5].

The Hodgkin-Huxley model solely describes the electrical aspect of a nerve pulse. It have been shown that the electrical pulse is coupled with a swelling of the membrane [47] (see Fig. (2.8), a), along with a change in internal pressure in the axon membrane [48]. The adiabatic nature of the nerve pulse combined with the mechanical changes and the physical size of the pulse, indicates that the nerves pulses could be a type of *sound wave*.

⁶In newer revisited versions of the HH-model the action potential is not only attributed to ion flows, though it is still the essential mechanism.

This deduction lead to the proposal of the Soliton model by Heimburg and Jackson in 2005 [3].

2.2.2 Soliton Model

As part of the classical physical approach, there is a general consensus that when trying to explain a phenomena the explanation should be of the same length scales as the characteristic length scale of the phenomena – trying to explain waves on water based on molecular interaction is an impossible task. With this and the unexplained experimental findings in mind, Heimburg and Jackson [3] proposed that nerve signals are localized density waves (soliton)⁷, relaying their theory on thermodynamics and hydrodynamics. A soliton is a localized wave packet that has a constant shape and amplitude as it propagates. For the existence of solitary waves the medium has to display non-linearity and dispersion, which chancels one another. With non-linearity is meant that the speed of sound is a non-linear function of density and dispersion is the frequency dependency of the speed of sound. In the vicinity of the lipid melting transition the lipid membrane met both of these requirements.

The Soliton model is based on the equation of sound. By assuming the nerve axon is a infinitely long homogeneous cylinder, the 3-dimensional geometry of the nerve axon degenerate into a 1-dimensional problem. The 1-dimensional equation of sound can be written as,

$$\frac{\partial^2}{\partial t^2} \Delta\rho^A = \frac{\partial}{\partial x} \left(c^2 \frac{\partial}{\partial x} \Delta\rho^A \right), \quad (2.7)$$

where $\Delta\rho^A(x, t) = \rho^A(x, t) - \rho_0^A$ ⁸ is the lateral density of the nerve membrane and c is the speed of sound also referred to as the phase velocity. As illustrated in Fig. (1.2) (in the [Introduction](#), chapter 1), the phase velocity in plane of the lipid membrane is a non-linear function of density in the vicinity of the lipid melting transition. To capture the non-linear behavior, Heimburg and Jackson expand the squared phase velocity into a power series to second order

$$c^2 = c_0^2 + p(\Delta\rho^A) + q(\Delta\rho^A)^2 + \dots, \quad (2.8)$$

where c_0 is the phase velocity in the fluid phase, far from the transition. $p < 0$ and $q > 0$ are the taylor expansion coefficients which are determined

⁷Recently experiments have verified the existence of lateral density solitons in quasi 2-dimensional sheets [49].

⁸ ρ_0^A is the lateral density of the membrane in the fluid phase and is used as the zero point for the lateral density.

from the density dependent phase velocity of a given considered system⁹. Experimentally it is very difficult to probe the frequency dependence of the phase velocity below $kH\text{z}$ ¹⁰. Having no detailed data on the frequency dependence of the phase velocity at low frequencies, Heimburg and Jackson chose the dispersion term to take the simplest possible form ($-h \frac{\partial^4}{\partial x^4} \Delta\rho^A$), resulting in the final formulation of the model

$$\frac{\partial^2}{\partial t^2} \Delta\rho^A = \frac{\partial}{\partial x} \left((c_0^2 + p(\Delta\rho^A) + q(\Delta\rho^A)^2) \frac{\partial}{\partial x} \Delta\rho^A \right) - h \frac{\partial^4}{\partial x^4} \Delta\rho^A, \quad (2.9)$$

where $h > 0$ is the dispersion constant.

The low-amplitude periodic solution of Eq. (2.9) ($c = c_0$) has the form $\Delta\rho^A = \rho_0^A \exp(i\omega(t - x/v))$, where v is the velocity of the soliton (group velocity). Inserting this expression into Eq. (2.9) the group velocity takes the form:

$$v^2 = c_0^2 + hk^2 \approx c_0^2 + h \frac{\omega^2}{c_0^2} \quad (2.10)$$

This approximation holds for $v \approx c_0$, using $k \equiv \omega/v$. From Eq. (2.10) it is clear that the dispersion constant acts as the taylor expansion coefficient of the second order term of the frequency dependent phase velocity, around $\omega = 0$. The sign of the frequency is of no importance since it is only represents a phase shift, meaning that the phase velocity must be an even function of frequency. By this argument the chosen dispersion term truly poses the simplest meaningful choice, as the lowest order, non-trivial, expansion of the phase velocity's frequency dependence.

Assuming that the general solution to Eq. (2.9) propagates with a constant velocity ($z = x - vt$, where $v \leq c_0$), is localized and vanishes for $|z| \rightarrow \infty$, it can be solved analytically [50]:

$$\Delta\rho^A(z) = \frac{p}{q} \frac{1 - \left(\frac{v^2 - v_{min}^2}{c_0^2 - v_{min}^2} \right)}{1 + \left(1 + 2\sqrt{\frac{v^2 - v_{min}^2}{c_0^2 - v_{min}^2}} \cosh \left(\frac{c_0}{h} z \sqrt{1 - \frac{v^2}{c_0^2}} \right) \right)}, \quad (2.11)$$

where $v_{min} = \sqrt{c_0^2 - \frac{p^2}{6q}}$ is the minimum group velocity. This type of localized solution is referred to as solitary wave or simply soliton and is the namesake of the model. From Eq. (2.11) it can be seen that the solution is symmetric around the top point, and that the width of the soliton scales

⁹For LUV of DPPC at $T = 318.15\text{ K}$ the parameters takes the values $\rho_0^A = 4.035 \cdot 10^{-3}\text{ g/m}^2$, $c_0 = 176.6\text{ m/s}$, and the expansion coefficients: $p = -16.6 \cdot c_0^2/\rho_0^A$ and $q = 79.5 \cdot c_0^2/(\rho_0^A)^2$.

¹⁰Ultrasonic experiments can commonly probe a frequency regime from $k\text{Hz}$ to $G\text{Hz}$.

with the dispersion constant. Heimburg and Jackson chose $h = 2 \text{ m}^4/\text{s}^2$, based on the physical length (distance) of measured nerve pulses. Using this value, the Soliton model predicts a minimum velocity of solitons in DPPC membranes to be $v_{min} \approx 0.65 \cdot c_0 = 115 \text{ m/s}$ – a number which is very close to the pulse velocity measured in myelinated nerves. The minimum velocity corresponds to the maximum amplitude or density change of $\Delta\rho_{max}^A / \rho_0^A \approx 0.21$. Soliton profiles for a number of different propagation velocities are presented in Fig. (2.9).

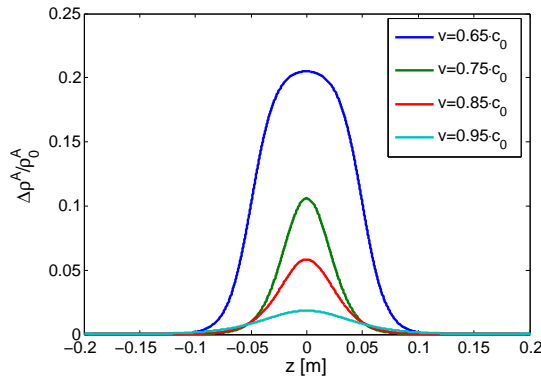


Figure 2.9: Soliton profiles for LUV of DPPC, for velocities between the lower limit $v = 0.65 \cdot c_0$ and $v = 0.95 \cdot c_0$. Profiles have been produced by numerical integration by the Euler method and have been mirrored around their top point.

Lautrup *et al.* [51] have shown that the Soliton model is stable over ranges of physical relevance (several meters) with respect to noise and heterogeneities in the membrane – which is essential for a model that describe a biological system. They further showed that the soliton can be produced (excited) by arbitrary localized non-solitonic excitation, meaning that any perturbation of a sufficient amplitude should be able initialize a soliton, and hereby a nerve pulse.

The soliton is locally pushing the lipid membrane into its lipid melting transition as it propagates. Remember that the state of the membrane is coupled to thickness, charge density, etc. and that these change drastically during the transition. This means that during the propagation the soliton will display a number of secondary effect such as geometric changes and changes in electrical properties, though the detailed nature of this coupling has yet to be worked out. The propagation of the soliton will result in changes in thickness of the membrane and also have a electrical component, both observed during the propagation of nerve signals. The most important feature of the Soliton model is its ability to predict the reversible heat changes in phase with the action potential. It should however be emphasized that the

present form of the Soliton model only describes nerve pulses in myelinated nerves where all propagation is kept in 1-dimension.

The essential feature of the membrane that makes propagation of solitons possible, is the existence of the lipid phase transition. As described in [Membrane Phase Transition](#) (section 2.1.3), there is a great number of “handles” by which the transition can be influenced. Among these handles are general anesthetics. Based on this Heimburg and Jackson have made a number of prediction about the nature of anesthetics [11].

At present the low frequency dispersion behavior of lipid membranes is unknown. The exploration of the dispersion of sound in lipid membranes is essential to the justification of the thermodynamical approach to nerve pulses and the Soliton model.

2.3 Sound

In 1816 Laplace corrected the calculations done by Newton of the velocity of sound, by stating that sound propagation is an adiabatic process. Meaning that a sound wave (density wave) in a fluid is followed by local temperature variations. Stokes (1845) [52] and Kirchhoff (1868) [53] extended the theory, by including absorption due to internal friction and heat conduction. In 1928 Herzfeld and Rice [54] extended the theory of sound further, by introducing a finite transfer rate between different degrees of freedom, which can lead to hysteresis and dissipation.

The goal of this section is to introduce and familiarize the reader with propagation of sound on a basic level and extend this formalism to include complex phenomena such as dispersion and attenuation.

2.3.1 Introduction to Sound

The lipid membrane can in the *fluid* phase be considered to be a quasi two dimensional fluid whereas the *gel* phase share similarities with solids [17]. Sound can propagate in fluid as well as in solids, and that governing equation, the equation of sound, is universal. The generality of the equation of sound means that only the macroscopic thermodynamic properties of the system is important for the propagation of sound.

In its simplest form the *equation of sound* or the *wave equation* is formulated as follows¹¹:

$$\frac{\partial^2 \phi}{\partial t^2} + c^2 \nabla^2 \phi = 0 \quad (2.12)$$

where

$$c = \sqrt{\left(\frac{\partial p}{\partial \rho}\right)_S} = \frac{1}{\sqrt{\kappa_S \rho}} \quad (2.13)$$

is the speed of sound, or phase velocity, κ_S is the adiabatic compressibility and $\phi = \phi(x, t)$ is a scalar function. In context of the Soliton model the scalar function is the lateral density. A derivation of the equation of sound, based on fluid dynamics, is found in [Equation of Sound](#) (appendix B).

The general solution to the equation of sound, Eq. (2.12), has the form:

$$\phi = A \exp(i\omega(t - x/\hat{c})) \quad (2.14)$$

where ω is the angular frequency of the wave, x denotes the position of the wave, A is the amplitude and \hat{c} is the complex phase velocity of sound.

¹¹In the derivation of the equation of sound the two basic assumptions are: perturbation are small and that sound propagation is an adiabatic process.

The phase velocity of sound will for any real system be a complex quantity ($\hat{c} = Re(c) + iIm(c)$) due to the dispersion and absorption of sound in real mediums. The real part of the phase velocity will result in a phase shift of the wave (dispersion) and the imaginary part will result in a lowering of the amplitude or intensity of the sound over propagation distance (attenuation). This can clearly be seen by inserting the complex phase velocity into Eq. (2.14).

$$\phi = A \exp \left(i \left(\omega t - x \frac{\omega Re(c)}{Re(c)^2 + Im(c)^2} \right) \right) \exp \left(-x \frac{\omega Im(c)}{Re(c)^2 + Im(c)^2} \right) \quad (2.15)$$

The real and imaginary part of the phase velocity are coupled¹² so there can be no attenuation without some level of dispersion and the visa versa, which is illustrated in Fig. (2.10).

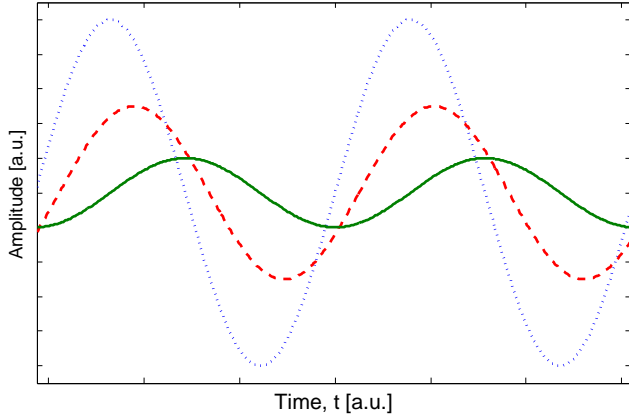


Figure 2.10: A illustration of solutions to Eq. (2.12) for three different complex phase velocities, where the *blue line* represent the ideal case (no attenuation and dispersion), the *red line* is some level of attenuation and dispersion and last the *green line* is with heavy attenuation and dispersion.

That the phase velocity is complex means that the adiabatic compressibility is a complex quantity [56]. The complex adiabatic compressibility will be referred to as the dynamic adiabatic compressibility. The dynamic adiabatic compressibility is only equal to the equilibrium adiabatic compressibility in the ideal case (no attenuation and dispersion).

¹²The real and imaginary part of the phase velocity are related through the *Kramers-Krönig relation* [55].

2.3.2 Effects that Distort the Propagation of Sound

Until this point the physical phenomena that result in dispersion and attenuation have not been discussed. This section is devoted to introducing these physical phenomena and their effect on the propagation of sound.

In 1928 Herzfeld and Rice [54] extended the theory of sound by arguing that internal vibrational modes of polyatomic molecules require time to come into thermal equilibrium with translational degrees of freedom. If the density (or pressure) perturbation is on the same timescale as these internal mean relaxation times or faster, the temperature response of the system will lag behind the perturbation, resulting in hysteresis and dissipation of sound.

Herzfeld and Rice considered three phenomena that effects the propagation of sound: Internal friction, heat conduction (introduced by Stokes (1845) [52] and Kirchhoff (1868) [53]) and their own addition, finite transfer rates between translational and internal degrees of freedom. In their view these phenomena affects the propagation of sound qualitatively as follows:

- *Internal friction* affect the propagation of sound by retarding movement, thereby elongating a given wave-length and increasing the phase velocity of the wave.
- *Heat conduction* is the medium's ability to transfer heat. The heat conducted during one period of the wave increase with frequency, due to the steepness of the temperature gradient. This will in effect lower the phase velocity with increasing frequencies.
- *Finite transfer rates* between translational and internal degrees of freedom will in effect keep the internal degrees freedom from taking up all the heat. This will decrease the effective heat capacity¹³ and increase the phase velocity with increasing frequencies¹⁴.

These effects predict in total an increase in the phase velocity of sound with increasing frequency. This approach fathered the modern description of sound and is the basis of understanding attenuation and dispersion. Beyond these, there has been added a number of “geometric” considerations to the theory of sound, such as orientations in the medium (e.g. nematic phases) and boundary effects, which will though not be considered in the present thesis.

From the basic concepts of Herzfeld and Rice any “event” that can dras-

¹³Note that the effective heat capacity will be referred to as the dynamic heat capacity.

¹⁴The coupling between the dynamic heat capacity and the phase velocity will be discussed in [Adiabatic Compressibility](#) (section 3.2).

tically alter the extent of these phenomena will have large effect on the attenuation and dispersion of sound in a given medium.

2.3.3 Sound Propagation near Phase Transitions

As discussed in [Membrane Phase Transitions](#) (section 2.1.3) the physical properties of a system can change drastically during a phase transition, which in accordance with the above can lead to distortion of sound propagation in the system.

In 1962 Fixman [57] applied the basic concepts from Herzfeld and Rice to describe the viscosity of critical mixtures. He was motivated by the intimate relation between viscosity and attenuation. Critical mixtures of fluids show a sharp second-order transition, which among other is signified by a critical slowing down of the relaxation rates of the order-parameters. He considered instead of rates between translational and internal degrees of freedom as Herzfeld and Rice, a *continuum of long-wavelength order-parameter fluctuations*. With this he made the connection between the “transfer rates” and relaxation rates of order-parameters in systems. The slow-down during a transition means a drastic change in relaxation rates, which will result in large changes in the dynamic heat capacity of the system and thereby the phase velocity. There can also be changes in internal friction and general heat conduction during a phase transition but these will be secondary effects, since these effects occur on very small length- and timescales [58,59].

From this, it is the slow down of the characteristic relaxation rate during the lipid melting transition that, for low frequencies, exclusively causes the dispersion of sound.

The slow-down during phase transitions meant historically that investigation of otherwise too fast relaxation rates became experimentally accessible with ultra sound. This led to a great interest in describing sound propagation in materials undergoing first and second-order transitions [60–62].

Kawasaki [60] and Kroll and Ruhland [61] share the approach in attempting to calculate the second viscosity coefficient (or ”bulk” viscosity). Ferrell and Bhattacharjee [62,63] have in their work added the idea of *dynamic scaling* (critical exponents). With this approach, they provide a scaling function of the frequency dependent dynamic heat capacity, from which they are able to calculate the speed of sound. Tanaka *et al.* [64] showed experimentally that the theory made by Ferrell and Bhattacharjee is applicable to the large frequency regime for classical binary mixtures, unlike many of the previous mentioned approaches. In 1997 the same authors [65] published a scaling theory (BF-theory) for the isotropic-to-nematic phase transition, which is classified as a weak first-order transition. The BF-theory was originally developed for the 3-dimensional isotropic-to-nematic phase transition but

Halstenberg *et al.* [58] showed both experimentally and theoretically that it could be applied to the lipid melting transition of lipid bilayers in the ultrasonic regime.

The experimental and theoretical findings of Grabitz *et al.* [18] showed however that the relaxation behavior throughout the full range of the lipid melting transition fits very nicely to a single exponential decay. This observation simplifies the dynamics of the main melting transition from dynamic scaling theory to the simple relaxation behavior of equilibrium fluctuations [66]. Responses of systems with this type of relaxation behavior are generally governed by linear response theory, introduced by Eigen [67]. Mitaku and Date [16] used in 1982 this approach to analyze the dispersion and attenuation of small DMPC¹⁵ vesicles in the ultrasonic regime, with poor correspondence between data and theory. A similar approach was used by Van Odsol *et al.* [17, 36] to analyze kinetics of different membranes phase transitions in the frequency regime 0.1 Hz to 150 Hz – with great agreement between result and theory. From these findings, the simple relaxation behavior seem insufficient to describe high frequency behavior, but for low frequencies it described the system behavior quite well. For the frequency regime of interest in this thesis additional complication of the simple single exponential relaxation seem beyond the scope.

¹⁵1,2-Dimyristoylphosphatidylcholin

Chapter 3

Analytic Approach

The primary goal of this thesis is to estimate the speed of sound in the plane of a lipid membrane as a function of frequency. Sound can in short be described as propagation of low amplitude density (or pressure¹) waves, which are directly coupled to a following temperature wave due to the adiabatic nature sound.

The propagation of sound can be approached in two ways; mechanically or through thermodynamics. These approaches are intimately related and can in many cases be considered as equivalents. The thermodynamics of lipid membranes have been explored extensively during the last decades and a number of phenomenological simplifications have been found. In this thesis, sound propagation will be considered from a thermodynamic perspective.

The beauty of thermodynamics is its ability to describe vastly complex system by relatively few macroscopic properties, temperature, pressure, heat capacity, etc. With the development of non-equilibrium thermodynamics [66, 67]² understanding and describing dynamics of complex systems has become possible and hereby sound propagation.

The first challenge of this thesis is to find the response of lipid membranes to sound at different frequencies. The response of a system to periodic pressure perturbations is, if the system has a finite relaxation time, a frequency dependent problem³. The frequency dependence of sound is further complicated by the adiabatic nature of sound. The second challenge is to find a relationship between the system's response and speed of sound in the membrane. When this is achieved, the speed of sound can be found along with its frequency dependence.

¹Density and pressure are in sound propagation intimately related, since they are the direct product of one another. Sound can be described by pressure waves as well as by density waves.

²Other authors contributing greatly is: Einstein, Prigogine, Greene, Callen, ect.

³See Perturbation Simulations (section 4.2.2) for numerical exploration of this problem

3.1 Adiabatic Pressure Perturbations

Sound is the propagation of a pressure wave that is followed by a temperature wave due to its adiabatic nature. From a thermodynamical point of view, these changes in pressure and temperature couple to a change in the heat of the system

$$dQ = c_P dT - L_P dP, \quad (3.1)$$

where dQ is the change in the heat of the system, c_P is the heat capacity and L_P is the latent heat of expansion, defined as $L_P = (dH/dP)_T - V$. Eq. (3.1) can be rewritten to the form [68]:

$$dQ = c_P dT - TV\alpha_P dP, \quad (3.2)$$

where $\alpha_P = -(\frac{dV}{dT})_p/V$ is the thermal expansion coefficient. A full derivation can be found in the appendix: C.1. Using the Maxwell relation, $(dV/dS)_V = (dT/dP)_S$,

$$\begin{aligned} TV\alpha_P &= -T \left(\frac{dS}{dT} \right)_P \left(\frac{dV}{dS} \right)_P \\ &= \left(\frac{dQ}{dT} \right)_P \left(\frac{dT}{dP} \right)_S \\ &= c_P \left(\frac{dT}{dP} \right)_S. \end{aligned} \quad (3.3)$$

The expression for the change in heat can now be written as

$$dQ = c_P(T, P) \left(dT - \left(\frac{dT}{dP} \right)_S dP \right). \quad (3.4)$$

Adiabatic is defined as no transfer of heat between the considered system and the outside, this is well approximated by the entropy of the system being constant. The entropy being constant means that the “position”⁴ in a phase transition is constant during the perturbations in pressure and temperature. Since the position in the transition is fixed the Clausius-Clapeyron relation⁵ can be used

$$\frac{dP}{dT} = \frac{\Delta H}{T\Delta V}, \quad (3.5)$$

where ΔH and ΔV are the enthalpy and volume changes associated to the transition, respectively. Note that these are constant system properties for a given transition. Inserting Eq. (3.5) into Eq. (3.4),

$$dQ = c_P(T, P) \left(dT - \left(\frac{T\Delta V}{\Delta H} \right) dP \right). \quad (3.6)$$

⁴By position is meant, the fraction of completion of the phase transition.

⁵The use of the Clausius-Clapeyron relation can be justified by the weak first-order nature of the lipid melting transition.

From this it is clear that the heat capacity acts as a transfer function that couples adiabatic changes in pressure to changes in heat. Using Eq. (3.6) the change in heat can be found by integration:

$$\int dQ = \int c_P(T, P) dT - \int c_P(T, P) \left(\frac{T \Delta V}{\Delta H} \right) dP \quad (3.7)$$

Until this point, the heat capacity is a constant system property and transfer rates have not been considered. In any real system transfer rates are finite and changes happen in finite time. Thus, the changes in pressure and temperature can be represented as rates:

$$\int dQ = \int c_P(t) \dot{T} dt - \int c_P(t) \left(\frac{T \Delta V}{\Delta H} \right) \dot{P} dt \quad (3.8)$$

Note that $T = T_{equilibrium}$ which holds in the approximation of small absolute changes in temperature, which is a standard assumption in propagation of sound.

If changes in pressure or temperature happen faster than the transfer rate (or relaxation rate) the energy transferred during this change will only be a part of the otherwise transferred amount. Considering Eq. (3.6), the finite transfer rate will potentially lower the effective transfer function, in this case the heat capacity⁶. This also means that the heat capacity must have a relaxation term, Ψ_{c_P} , and Eq. (3.8) must be written as a convolution:

$$\delta Q(t) = \int_{\infty}^t (c_P(\infty) + \Delta c_P (1 - \Psi_{c_P}(t - t'))) \left(\dot{T}(t') + \frac{T \Delta V}{\Delta H} \dot{P} \right) dt' \quad (3.9)$$

where $\delta Q(t)$ is the change in heat, $c_P(\infty)$ is the part of the heat capacity that relaxes at much greater rates than changes in pressure and temperature considered. In the lipid bilayer system $c_P(\infty)$ is the heat capacity contribution from lipid chains, often referred to as the background contribution. Δc_P is the part of the heat capacity which has relaxations rates comparable to the perturbations, in the lipid membrane system this is the excess heat capacity. In Eq. (3.9) it has been assumed that the mechanisms of relaxation are the same for pressure and temperature. This assumption has been justified experimentally and numerically in the literature [18, 33, 39, 69]. In the lipid melting transition changes in extensive variables are found to be proportional and having a common relaxation mechanism.

Eq. (3.9) can be rewritten using the convolution theorem and Fourier transformation to the form

$$\delta Q = c_P(\omega) \left(T(\omega) + \frac{T \Delta V}{\Delta H} P(\omega) \right), \quad (3.10)$$

⁶Note how this fits into the picture of the course of dispersion and attenuation of sound.

where,

$$c_P(\omega) = c_P(\infty) - \Delta c_P \int_0^\infty e^{i\omega t} \dot{\Psi}_{c_P}(t) dt. \quad (3.11)$$

In Eq. (3.10), $T(\omega)$ and $P(\omega)$ are assumed to be periodic (sinusoidal). The derivations are based on [17].

Note that no structural or system specifications have been used in the derivation, only the nature of the phase transition of the lipid bilayer. Note further that the frequency dependent heat capacity is a complex function, and will therefore be referred to as the dynamic heat capacity. All the above derivations can be carried out with lateral pressure instead of pressure, the choice of using pressure is entirely for convenience of notation. From Eq. (3.11) the frequency dependent transfer function (dynamic heat capacity)⁷ can be found, giving a full description of how the lipid bilayer respond to adiabatic pressure perturbations. $c_P(\infty)$ and Δc_P are both experimentally easily available and well known in the literature [39]. The only unknown factor is the relaxation function, Ψ_{c_P} . From the above consideration, the relaxation function must be related to the rate of energy transfer. The fluctuation-dissipation theorem ensures that the rates of energy transfer are equivalent to the relaxation behavior of the fluctuation of energy. Using that the heat capacity is a measure of the fluctuation of enthalpy, the relaxation function of the heat capacity must be the relaxation function of the enthalpy fluctuations [17]. In the lipid melting transition changes in volume, area and enthalpy are proportional functions, leaving only one independent fluctuating variable. This supports that the relaxation function for pressure and temperature being the same and that this relaxation function can be deduced from the enthalpy fluctuations.

Single relaxation rate

The relaxation behavior of the fluctuations of enthalpy in pure lipid vesicles has been considered theoretically, numerically and experimentally by Grabitz *et al.* [18]. They found that the relaxation of enthalpy is well described by a single exponential function,

$$(H - \langle H \rangle)(t) = (H - \langle H \rangle)(0) \cdot \exp\left(-\frac{t}{\tau}\right), \quad (3.12)$$

⁷It is important note the difference between the dynamic heat capacity (frequency dependent) and the normally known equilibrium heat capacity. The equilibrium heat capacity is a constant system property whereas the dynamic heat capacity is an effective heat capacity that can be lower or equal to the equilibrium heat capacity due to finite transfer rates in real systems.

where $(H - \langle H \rangle)(0)$ serves only as a proportionality constant and τ is the relaxation time. Note that this is a simple linear response function⁸. The authors further found that the relaxation time, for a number of different pure lipid membranes, is proportional to its respective excess heat capacity,

$$\tau = \frac{T^2}{L} \Delta c_P, \quad (3.13)$$

where L is a phenomenological coefficient. They found $L = 13.9 \cdot 10^8 J \cdot K / (s \cdot mol)$ for LUV of DPPC. Extensive numerical explorations of the relaxation behavior of the lipid melting transition can be found in [Relaxation Simulations](#) (section 4.2), including verification of the single exponential relaxation behavior, the proportionality relation and response of the lipid membrane to periodic perturbations. Beyond this, a theoretical validation of the single exponential relaxation behavior is shown in [Relaxation Time](#) (appendix A.2).

Using the relaxation function of the enthalpy fluctuation as the relaxation function of the dynamic heat capacity,

$$\Psi_{c_P} = \exp\left(-\frac{t}{\tau}\right), \quad (3.14)$$

Eq. (3.11) can be solved and the dynamic heat capacity can be found.

$$\begin{aligned} c_P(\omega) &= c_P(\infty) - \Delta c_P \int_0^\infty e^{i\omega t} \left(\frac{-1}{\tau}\right) e^{\frac{-t}{\tau}} dt \\ &= c_P(\infty) + \Delta c_P \left(\frac{1 + i\omega\tau}{1 + (\omega\tau)^2} \right) \end{aligned} \quad (3.15)$$

Note that all variables in the dynamical heat capacity are known quantities from experiments.

Van Osdol *et al.* [70] have made adiabatic pressure perturbation experiments on unilaminar and multilaminar vesicles made of DPPC. In these experiments they analyzed the relaxation behavior of the lipid membrane by measuring how the effective heat capacity and the compressibility change as a function of frequency. Though the data available for unilaminar vesicles is very limited and has large errors, it still illustrates the tendency of the effective heat capacity, which fits very nicely with the proposed functional form for the dynamic heat capacity. The adopted data and the fits are shown in Fig. (3.1).

⁸See [Linear Response](#) (appendix D) for a basic introduction to the concept and for visualization see [Perturbation Simulations](#) (section 4.2.2, results).

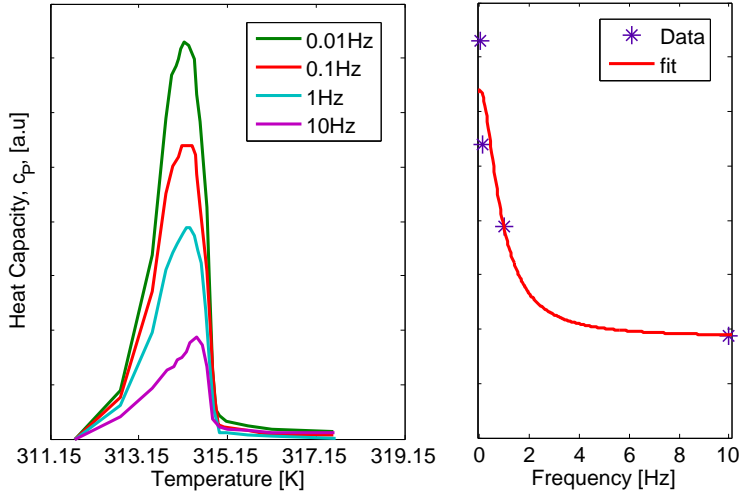


Figure 3.1: *Left:* Shows the heat capacity profiles for 4 different frequencies. *Right:* The top points from the heat capacity profiles have been fitted to the amplitude of the proposed dynamic heat capacity yielding an estimated relaxation time of about 0.18s. By amplitude is meant the amplitude of the polar form of the dynamic heat capacity where background contributions have not been taken into account. Data have been adopted from [70] and recalculated to the isobar heat capacity in accordance with theory, mentioned in the article. The errors on these plots are beyond proper estimation.

3.2 Adiabatic Compressibility

In the [Theory of Sound](#) (section: 2.12) it was noted that the dynamic heat capacity could be related to the phase velocity, though no remark was made as to how.

The adiabatic lateral compressibility is defined as

$$\kappa_S^A = \frac{1}{\langle A \rangle} \left(\frac{d \langle A \rangle}{d \Pi} \right)_S, \quad (3.16)$$

where Π is the lateral pressure. Using the Maxwell equations [68] the adiabatic lateral compressibility can be rewritten to

$$\kappa_S^A = \kappa_T^A - \frac{T}{\langle A \rangle c_P^{system}} \left(\frac{d \langle A \rangle}{dT} \right)_\Pi^2, \quad (3.17)$$

where

$$\kappa_T^A = \frac{1}{\langle A \rangle} \left(\frac{d \langle A \rangle}{d \Pi} \right)_T = \kappa_T^A(\infty) + \frac{\gamma_A^2 T}{\langle A \rangle} \Delta c_P. \quad (3.18)$$

In the last equality the experimentally found phenomenological proportionality between ΔH^{ex} and ΔA^{ex} (Eq. (2.4)) has been used [33]. $\kappa_T^A(\infty)$ is the part of isothermal lateral compressibility of the lipid membrane that relaxes at much greater rates than changes in the pressure and temperature considered. c_P^{system} is the heat capacity of the total thermodynamical system.

In the literature [65, 71] on attenuation and dissipation of sound in critical mediums a rewritten version of Eq. (3.17) is often used to relate the dynamic heat capacity to the adiabatic compressibility. This can be done in a straight forward manner, by deploying the Pippard-Buckingham-Fairbank relations (PBFR) [72, 73]. These are a number of relations that state, that close to a first or second order phase transition the critical phenomena will dominate the behavior of the system, leading to linear relationships between the relevant susceptibilities. The experimentally found phenomenological proportionalities verifies the validity of the PBFR in the lipid membranes since these pose an even stronger relationship, proportionality over linearity. The issue of this approach is that the heat capacity that goes into Eq. (3.17) is that of the total system. In the mentioned literature the medium in consideration takes up the full system, whereas in the lipid membrane system a pseudo 2-dimensional system (the bilayer) embedded in a full 3-dimensional system is considered, making the total system heat capacity a complicated variable.

The total thermodynamical system in consideration in this project is made up of a water reservoir containing large unilaminar lipid vesicles. These vesicles being large, justifies the assumption that there are no bending effects and that they contain enough water for the properties of the two sides of the bilayer to be identical. Using these assumptions, the thought experiment system is but one layer of the lipid bilayer (membrane) that through the head group is connected to a water reservoir. Imagine a standing temperature wave in the bilayer. The transfer of heat from the wave to the surrounding water will be time dependent. Approaching $\omega \rightarrow 0$, the amount of water (heat reservoir) participating will effectively go to infinity. In the other extreme, ($\omega \rightarrow \infty$), no heat will be transferred to the surrounding water reservoir. These considerations in effect lead to having the heat capacity of the total system to be frequency dependent. This was proposed by Halstenberg *et al.* [69] and was used by Heimburg and Jackson [3], where they were able to make nice predictions regarding the experimentally found high frequency limit and the low frequency limit using Eq. (3.17), where

$$c_P^{system}(\omega) = c_P^{lipid} + c_P^{reservoir}(\omega). \quad (3.19)$$

$c_P^{lipid} = \Delta c_P + c_P(\infty)$ is the complete heat capacity (in equilibrium) of the lipid membrane. $c_P^{reservoir}(\omega)$ is the heat capacity of the participating heat

reservoir. In this approach it is the size of the heat reservoir that is frequency dependent. The wanted relationship between adiabatic lateral compressibility and frequency is somewhat contained within the dynamic heat capacity. If the considered medium were spanning the full thermodynamical system, the dynamical heat capacity would be the heat capacity of the full system. When the dynamic heat capacity now is only the effective heat capacity of the membrane and not the full system, how does this relate to the adiabatic lateral compressibility? Within this question is the question of how a finite heat reservoir affects the effective heat capacity of the membrane. If such a relation could be established, the dynamic heat capacity could be used to describe the frequency dependency of the heat reservoir and thereby the frequency dependency of the adiabatic lateral compressibility.

Using the proportionality relation between ΔH^{ex} and ΔA^{ex} (Eq. (2.4)) in Eq. (3.17) and assuming that the changes in area, as a function of temperature in the phase transition region, are completely dominated by the transition associated change in area, the following approximation can be made [69]:

$$\begin{aligned}\kappa_S^A &\approx \kappa_T^A(\infty) + \frac{\gamma_A^2 T}{\langle A \rangle} \Delta c_P - \frac{\gamma_A^2 T}{\langle A \rangle} \frac{(\Delta c_P)^2}{c_P^{system}} \\ &= \kappa_T^A(\infty) + \frac{\gamma_A^2 T}{\langle A \rangle} \left(\Delta c_P - \frac{(\Delta c_P)^2}{c_P^{system}} \right).\end{aligned}\quad (3.20)$$

The nature of the last parenthesis is unknown, though it has the unit of a heat capacity. Posed at this point as an ansatz,

$$c_P^{effective} = \Delta c_P - \frac{(\Delta c_P)^2}{c_P^{system}}, \quad (3.21)$$

is the effective heat capacity of the lipid membrane in a adiabatically isolated heat reservoir. Based on the ansatz and the argument that leads to Eq. (3.19), the effective heat capacity must be the dynamic heat capacity. From this, the dynamic heat capacity can be related directly to the adiabatic lateral compressibility through Eq. (3.20):

$$\kappa_S^A = \kappa_T^A(\infty) + \frac{\gamma_A^2 T}{2 \langle A \rangle} \cdot \Delta c_P(\omega), \quad (3.22)$$

where the $\Delta c_P(\omega)$ is the dynamic heat capacity without background. The factor of 2 is due to Eq. (3.20) being the adiabatic lateral compressibility of a single monolayer. Since the area is an extensive variable the compressibility of the bilayer is half of that of a monolayer. A justification of the ansatz will be made in [Finite System Simulations](#) (section 4.3).

3.3 Speed of Sound

Assuming the posed ansatz (Eq. (3.21)) to be true, it is possible to relate the dynamic heat capacity to the frequency dependent adiabatic lateral compressibility of the lipid membrane. From the adiabatic lateral compressibility (Eq. (3.22)) the lateral phase velocity (c^A) can be found using Eq. (2.13):

$$c^A = \frac{1}{\sqrt{\kappa_S^A \rho^A}}$$

The frequency dependent adiabatic lateral compressibility, κ_S^A , is complex and will be referred to as the dynamic compressibility, κ^A , for simplicity of notation. The lateral phase velocity is a complex quantity: The real part is associated to the dispersion and the complex part results in attenuation. The goal of this thesis is to estimate the dispersion in lipid membranes, being the real part of the lateral phase velocity. For this, the real part of the lateral phase velocity squared can be isolated as follows:

$$\operatorname{Re}(c^A) + i\operatorname{Im}(c^A) = \frac{1}{\sqrt{\rho^A (\operatorname{Re}(\kappa^A) + i\operatorname{Im}(\kappa^A))}} \Rightarrow \quad (3.23)$$

$$\operatorname{Re}(c^A)^2 = (\rho^A)^{-1} \left(\frac{\operatorname{Re}(\kappa^A) + \sqrt{\operatorname{Re}(\kappa^A)^2 + 4\operatorname{Im}(\kappa^A)^2}}{2(\operatorname{Re}(\kappa^A)^2 + \operatorname{Im}(\kappa^A)^2)} \right), \quad (3.24)$$

where

$$\operatorname{Re}(\kappa^A) + i\operatorname{Im}(\kappa^A) = \left(\kappa_T^A(\infty) + \frac{\gamma_A^2 T}{2 \langle A \rangle} \operatorname{Re}(\Delta c_P(\omega)) \right) + i \left(\frac{\gamma_A^2 T}{2 \langle A \rangle} \operatorname{Im}(\Delta c_P(\omega)) \right), \quad (3.25)$$

and $\Delta c_P(\omega)$ is the phase transition associated part of the dynamic heat capacity. The derivation leading to the functional form of Eq. (3.24) is carried out in detail in [Real Part of the Phase Velocity](#) (appendix C.2).

By inserting Eq. (3.15) into Eq. (3.25) the squared real part of lateral phase velocity, Eq. (3.24), takes the form:

$$\operatorname{Re}(c^A)^2 = \frac{\frac{1}{c_1^2} + \frac{1}{c_2^2} \frac{1}{(1+(\omega\tau)^2)} + \sqrt{\left(\frac{1}{c_1^2} + \frac{1}{c_2^2} \frac{1}{(1+(\omega\tau)^2)} \right)^2 + 4 \left(\frac{1}{c_2^2} \frac{\omega\tau}{(1+(\omega\tau)^2)} \right)^2}}{2 \left(\left(\frac{1}{c_1^2} + \frac{1}{c_2^2} \frac{1}{(1+(\omega\tau)^2)} \right)^2 + \left(\frac{1}{c_2^2} \frac{\omega\tau}{(1+(\omega\tau)^2)} \right)^2 \right)}, \quad (3.26)$$

where for the convenience of notation,

$$c_1^2 \equiv (\rho^A \kappa_T^A(\infty))^{-1} \quad (3.27)$$

and

$$c_2^2 \equiv \left(\rho^A \frac{\gamma_A^2 T}{2 \langle A \rangle} \Delta c_P \right)^{-1}, \quad (3.28)$$

recognizing c_1 as the background lateral phase velocity and c_2 as the lateral phase velocity component related to the lipid melting transition.

The limiting cases predicted by Eq. (3.26) is the same as predicted by Heimburg and Jackson [3]:

$$\omega\tau \rightarrow 0: \quad Re(c^A)^2 = \left(\frac{1}{c_1^2} + \frac{1}{c_2^2} \right)^{-1}$$

$$\omega\tau \rightarrow \infty: \quad Re(c^A)^2 = c_1^2$$

In the low frequency limit the phase transition associated contribution on the phase velocity is fully accounted for, whereas in the high frequency limit the phase transition associated contribution disappears.

The dynamic heat capacity (Eq. (3.15)) is based on the relaxation behavior of the system to be well described by a single exponential. This single exponential relaxation behavior poses the simplest possible frequency dependence of the lateral phase velocity imaginable – often referred to as a *Debye term* in the ultrasonic field. The lipid membrane system is special in its pseudo 2-dimensional nature and the solution can therefore not be considered trivial. Despite the simplicity of this approach, it should still be possible to make a good estimate of the lipid membrane's behavior in the low frequency range.

Due to the found analytic form of Eq. (3.26) not only the phase velocity limits are accessible. The area, the lateral density and the background isothermal compressibility are all directly proportional to the fluid fraction⁹ [39]. Using the proportionality relation Eq. (3.13) the relaxation times can be found from the excess heat capacity. Then, Eq. (3.26) can be solved from the excess heat capacity and the fluid fraction, see Fig. (3.2).

The excess heat capacity and fluid fraction used have been found by Monte Carlo simulations using the Doniach model, see [Simulation of the Doniach Model](#) (section 4.1.4).

⁹The fluid fraction is the fraction of a considered lipid system that is in the fluid phase.

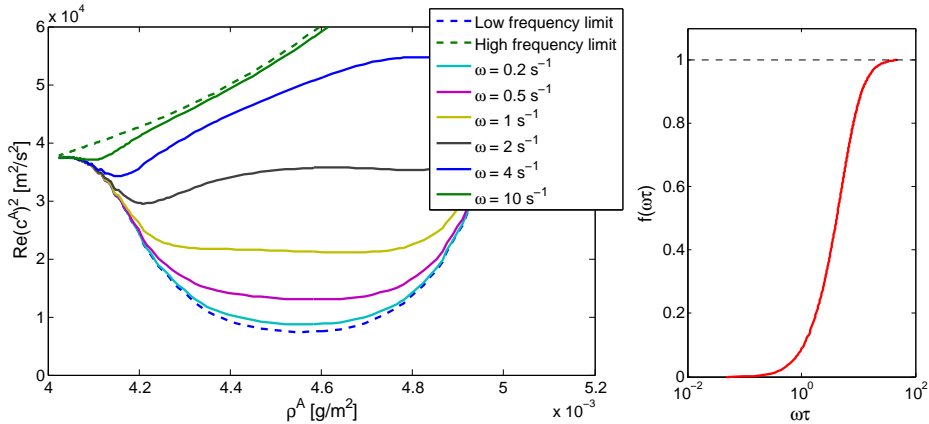


Figure 3.2: *Left:* The real part of the lateral phase velocity squared as a function of density at different angular frequencies along with the limiting cases: $\omega \rightarrow 0$ and $\omega \rightarrow \infty$. The calculations of the lateral phase velocity is based on single exponential relaxation behavior. *Right:* The generic function, $f(\omega\tau)$, that takes the phase velocity, at a given lateral density, from the low frequency limit ($f(\omega\tau) = 0$) to the high frequency limit ($f(\omega\tau) = 1$).

As is clearly indicated by Fig. (3.2) the real part of the phase velocity is estimated to depend very strongly on frequency. This is expected from the data of Van Osdol *et al.* [70] (Fig. (3.1)). However, a number of experiments have been conducted, probing the phase velocity in vesicles of DPPC with ultrasound [16, 69, 74]. In all these experiments some degree of the phase transition associated dip in phase velocity, even in the *MHz* regime, is observed. This is in disagreement with the posed estimate, which converges towards the high frequency limit long before the *kHz* regime. For high frequencies a number of effects has to be considered, in regard to this apparent discrepancy. As noted in [Sound Propagation near Phase Transitions](#) (section 2.3.3), there are secondary effects such as internal friction and general heat conduction that can have a phase transition component, which becomes accessible in the ultrasonic regime. This however does not fully explain the discrepancy between the high and low frequency behavior of the relaxation. From this, estimates of Eq. (3.26) at frequencies of order of magnitude faster than the relaxation times should, as previously noted, be used with care.

3.4 Dispersion

The goal of the project is to estimate the frequency dependency of the lateral phase velocity (estimate the dispersion). In the Soliton model for nerve signals, the dispersion has been considered to be small and only the first order term of the lateral phase velocity's frequency dependence has been considered.

$$(c^A)^2 = c_0^2 + hk^2 \approx c_0^2 + \frac{h\omega^2}{c_0^2}, \quad (3.29)$$

where the approximation holds for $c^A \approx c_0$ using $k \equiv \omega/c$.

From the estimate (Eq. (3.26)) of the squared lateral phase velocity, the dispersion constant, h , can be estimated by Taylor expanding around $\omega = 0$ to second order.

$$\begin{aligned} Re(c^A)^2 &\approx \left(\frac{1}{c_1^2} + \frac{1}{c_2^2} \right)^{-1} + \frac{1}{c_2^2} \left(\frac{1}{c_1^2} + \frac{1}{c_2^2} \right)^{-2} \tau^2 \omega^2 \\ &= c_0^2 + \frac{c_0^4}{c_2^2} \tau^2 \omega^2, \end{aligned} \quad (3.30)$$

where

$$\frac{1}{c_0^2} = \frac{1}{c_1^2} + \frac{1}{c_2^2}. \quad (3.31)$$

From this the dispersion constant takes the form:

$$h = \frac{1}{c_2^2} \left(\frac{1}{c_1^2} + \frac{1}{c_2^2} \right)^{-3} \tau^2 = \frac{c_0^6}{c_2^2} \tau^2 \quad (3.32)$$

The estimated dispersion constants are shown in Fig. (3.3), calculated from numerically found system variables.

The estimated dispersion constant is a function of density (or temperature), spanning a value range from 10^2 outside the phase transition to 10^8 at the peak of the phase transition. The dispersion constant density dependents is justified by the lateral phase velocity's strong relation to both the excess heat capacity and the relaxation rate. Note that the presence of the non-phase transition associated compressibility, $\kappa^A(\infty)$, effectively lowers the estimated dispersion constant.

Heimborg and Jackson [3] estimated the dispersion constant $h = 2 \text{ m}^4/\text{s}^2$ based on the physical width of a nerve pulse. The here found estimate of dispersion in a lipid membrane of DPPC differs very much from their estimate. Heimborg and Jackson have however showed that lung surfactant display squared phase velocity limits similar to that of DPPC membranes and it is

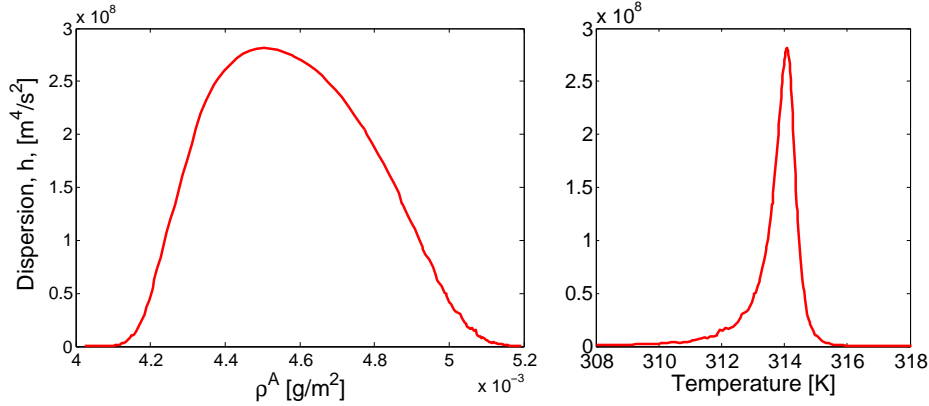


Figure 3.3: *Left:* The dispersion constant estimates base on a single exponential relaxation, as a function of density. *Right:* Same as to the left just as a function of temperature for illustration.

reasonable to assume relaxation times that are of the order of a hundred times slower. This would mean a lowering of estimated dispersion constant of 10^4 , assuming that used relations hold for the more complicated system of biological membranes. Taking this into account along with the density dependence of the dispersion constant, the estimated dispersion seem realistic in regard to the Soliton model.

Chapter 4

Simulations

Simulations are used to explore the thermodynamic properties of the main melting transition of lipid membranes, including the relaxation dynamics. In exploring the dynamics of the lipid membrane, a perturbation model extension¹ is introduced. With this model extension, the response of a lipid membrane to periodic perturbations is explored. In the course of the [Adiabatic Compressibility](#) (section 3.2) an ansatz was made regarding the heat capacity of the lipid membrane in a adiabatically isolated heat reservoir. In the pursuit of exploring the behavior of such a finite system, a model extension is here proposed and explored.

Starting out, the basic lipid membrane model is introduced along with the simulation methods used.

4.1 Modeling of Membranes

Phospholipid vesicles are important as models for biological membranes. In these artificial membranes general properties of lipid membranes can be studied in a reasonably well-defined system. Theoretically, mainly two classes of models have been proposed to describe the phase transition behavior of these phospholipid bilayer systems: One being phenomenological models, e.g. based on Landau theory, and the other being statistical mechanical microscopic models. The models used in the simulations of this thesis will be of the second class.

4.1.1 Doniach Model

A lipid membrane can be modeled using the molecular interaction (molecular dynamics simulation), but also coarse grain modeling is possible. The level

¹By model extension is meant that these are models extending a existing lipid membrane model.

of simplification of a given model should reflect the level of detail needed. Beyond this, the computational limitations on the number of states that can be explored during a simulation, sets a natural limit for system size and time frame. The lipid melting transition has been shown to be the collective behavior of hundreds of lipids [75], having relaxation time as slow as seconds [18]. The length and time scale of the lipid melting transition strictly limits the detail level of the potential models. Models like molecular dynamics (MD) simulations are both on length and time scale off by many orders of magnitude. The specific form of the model for the lipid membrane used in this thesis was proposed by Ivanova *et al.* [76]. This model is based on the model proposed by Doniach [77] and will therefore be referred to as the Doniach model. The Doniach model is conceptually based on the famous Ising model [78].

The Ising model is essentially a two state model that only takes nearest neighbor interactions into account, originally made for describing transition in ferromagnets. The Ising Hamiltonian in the original form is given by

$$\mathcal{H} = -\frac{\epsilon}{2} \sum_{\langle i,j \rangle} \sigma_i \sigma_j - g \sum_i \sigma_i, \quad (4.1)$$

where $\sigma_i = \pm 1$ are the allowed state values. The first sum is over nearest neighbors, indicated by $\langle i,j \rangle$, and ϵ is the nearest neighbor interaction parameter. The first sum accounts for the cooperative behavior of the system and in effect the possibility of a phase transition. The last sum takes into account the influence of an external field, where g denotes the strength and interaction with this applied field.

The Doniach model compared to more detailed models, such as the 10-state Pink model [79], is 100-1000 times faster and it has been shown that the choice of model has no significant effect on the overall physical behavior of the system [80]. This can be attributed to the extent of the cooperative nature of the transition, which makes the detailed single lipid model superfluous. Furthermore, the Doniach model contains only a few parameters, which can be determined through calorimetric experiments [76].

The following assumptions are needed for describing the lipid melting transition with the Ising model [77, 81].

- Each lipid can only be in one of the two following states:
 - A gel state with low enthalpy, H_g , and low entropy, S_g .
 - A fluid state with high enthalpy, H_f , and high entropy, S_f .
- The lipids only interact with nearest neighbors. This is justifiable since the majority of interactions between lipids are attributed to Van Der Waals interactions, which fall off according to $\frac{1}{R^5}$.

- All lipids, independent of state, are hexagonally packed (2D), meaning that each lipid molecule has $N_z = 6$ nearest neighbors. Experiments have shown that lipid membranes, mainly in the gel state have this packing [27, 82]. For simplicity we assume that the lipids in the fluid state are similarly packed².

These assumptions lead to the following Gibbs free energy [11]:

$$G = G_g + N_f (\Delta H - T \Delta S) + N_{fg} \omega_{fg}. \quad (4.2)$$

G_g denotes the Gibbs free energy of the system when all lipids are in the gel state. ΔH and ΔS are the changes in enthalpy and entropy between the gel and fluid states, respectively. N_f is the number of lipids in the fluid state and N_{fg} is the number of interactions between gel and fluid state lipids. ω_{fg} is the interaction parameter between gel and fluid state lipids.

The two parameters, ΔH and ΔS , can be found by calorimetric measurements, leaving the cooperativity parameter ω_{fg} as a free parameter. The free parameter is estimated by fitting the simulated heat capacity curves to the experimentally obtained ones. It is important to note that the model assumes that the two layers in the bilayer structure are completely uncoupled. It has lately been shown experimentally that the layers are in fact coupled and independent domain formations in the separate layers are not or rarely found [83]. This however does not pose a problem in the present thesis since no detail information is needed about the separate layers and the coupling is indirectly included in the fitted cooperativity parameter ω_{fg} .

This model has been used with success to model the lipid melting transition in lipid membranes, both pure lipid systems and including additional components, such as peptide (Gramicidin A) [84] or anaesthetics [85]. The main feat of interest of the Doniach model is its ability to model the relaxation behavior of the lipid melting transition in the single lipid membrane systems [18]. This ability enables the investigation of the dynamical properties of the lipid membrane.

²This assumption and its justification has been discussed in the literature [77].

4.1.2 Monte Carlo Method

The Monte Carlo method is a numerical method for exploring properties of statistical mechanical models.

Though the field of statistical mechanics is very well developed and elegant, most models are difficult to solve analytically – in many cases it is impossible. Consider a system containing N particles, which can be in one of two states. For this system the total number of states will be 2^N . For a small system containing only $N = 100$, the number of states will be $2^{100} \simeq 10^{30}$. In many cases the number of states can be degenerated, simplifying the problem, but the task of exploring such a state space³ is still often a cumbersome job. The computational capacities of computers have aided greatly in the field’s explorations. Though even with the great computational capacities of modern computers a brute force exploration of state space can be an impossible task. Methods have thus been developed to explore state space in an efficient manner. Each state in a system has a specific probability in a given thermodynamic, but commonly only a tiny fraction of states are very likely⁴. From this, sampling over a small fraction of states, can result in accurate estimations of physical properties. The Monte Carlo method is a method to, in an efficient way, sample the most likely states of a system.

The basic scheme of the Monte Carlo method is to use Markov processes as the generating engine. A Markov process is a process that given a state μ generates a new state ν of the system in a random fashion. The probability of generating the state ν given μ is called the transition probability $p(\mu \rightarrow \nu)$. The transition probability must not vary over time, and the transition probability must only depend on the properties of μ and ν , and not on any state the system previously has passed through. This ensures that the probability of generating ν given μ is conserved. Furthermore, it is demanded that it is possible to reach any state, from a given state, through a finite number of iterations, and that the transition probability from $\mu \rightarrow \nu$ is equal to the transition probability from $\nu \rightarrow \mu$. By doing this repeatedly a Markov chain of states that complies with conditions of ergodicity and detailed balance is generated. This scheme ensures that independent of starting state, it will eventually generate a succession of states that has the probability given by the Boltzmann distribution. The process of reaching the Boltzmann distribution is called “equilibration” due to its direct analog to the processes a real system goes through to equilibrate [86].

³A mathematical space, made up of the possible states of a system.

⁴An example not falling in this category is a system where the temperature goes to infinity, resulting in all states of the system becoming equally likely.

Rejection Algorithm

The goal of the Monte Carlo method is to explore the state space of a system in an efficient manner. This is done by applying a *rejection algorithm*.

Given a state, the Markov process will generate a new state, accompanied by a transition probability. The rejection algorithm is used to calculate the transition probability, such that the most likely states will have a higher chance to be generated, hereby making the search for the most likely states more efficient.

Over the years a number of different rejection algorithms have been proposed. They range in efficiency and other properties. The first and the most famous is the Metropolis algorithm [87]:

$$A(\mu \rightarrow \nu) = \begin{cases} \exp(-\Delta G/RT) & \text{if } \Delta G > 0 \\ 1 & \text{otherwise} \end{cases} \quad (4.3)$$

Where $A(\mu \rightarrow \nu)$ is the acceptance ratio, R is the gas constant, T is the temperature, and ΔG is the difference in free energy between state μ and ν . The acceptance ratio is related to the transition probability,

$$p(\mu \rightarrow \nu) = g(\mu \rightarrow \nu) A(\mu \rightarrow \nu) \quad (4.4)$$

where $g(\mu \rightarrow \nu)$ is the selection probability, the probability that a given change is selected.

The choice of rejection algorithm should reflect the features of interest in a given system. The Metropolis is a very efficient algorithm in general, both in the vicinity of a phase transition and away from it⁵. In the Metropolis and other single-flip algorithms the “time” it takes to simulate one correlation time scales with system size. By single-flip algorithm is meant an algorithm that only allows the flip of a single state in the system at a time. Another group of algorithms is cluster algorithms, e.g. the Wolff algorithm. In cluster algorithms the collective flipping of a cluster of, in the present context, lipids is considered. For this group of algorithms the “time” used to simulate one correlation time scales with cluster size⁶.

As previously mentioned, other factors than simulation speed plays a role in selecting the right rejection algorithm for a given problem. The simulation efforts of this thesis cover both exploration of the thermodynamical properties of the lipid melting transition and the associated dynamical properties. Due to this diversity in simulation efforts, the Glauber algorithm has

⁵In the phase transition the number of likely states blows up and covers a large number of states.

⁶For greater details on different rejection algorithms see [86].

been chosen [88]. The Glauber algorithm, sometimes referred to as the “heat bath” algorithm, is a very stable and robust single-flip algorithm that can be deployed both in and outside the phase transition region. This algorithm is slower than the Metropolis algorithm, but it mimics the state change kinetics seen in nature very well. It has been used by Grabitz *et al.* [18] to successfully simulate the relaxation kinetics of lipid membranes (DPPC) in the lipid melting transition.

The acceptance ratio for a given state change using the Glauber algorithm,

$$A(\mu \rightarrow \nu) = \frac{\exp(-\Delta G/RT)}{1 + \exp(-\Delta G/RT)} \equiv \frac{K}{1 + K}, \quad (4.5)$$

where K is the equilibrium constant.

The weighting of states using a rejection algorithm ensures that mainly the most relevant states are reached in finite iterations (Monte Carlo cycles). Common for all rejection algorithms is that the Monte Carlo simulation can reach all states in the system in finite time, for a finite system. This ensures, by the ergodic theorem [11], that averaging over one system for a long period of time is equal to averaging over a large number of snapshots of independent systems, making Monte Carlo simulations a powerful tool for estimating the properties of a statistical model.

4.1.3 Implementation of the Simulation

The goal of using the Monte Carlo method is to explore the important part of state space of a given model. This is done by constructing a series (a Markov chain) of configurations (states), which goes towards the most likely states of the system.

The Markov chain is generated using the following general scheme:

1. Given a system configuration, S_1 , a trial move is proposed to the configuration, S_2 . In this implementation only single flips of lipid states are considered, meaning that S_2 will only differ from S_1 by a flip of a single lipid.
2. The change in the Gibbs free energy associated to the proposed flip is calculated by the Doniach model (Eq. (4.2)). From this, the acceptance ratio, $A(S_1 \rightarrow S_2)$, can be found using the Glauber algorithm (Eq. (4.5)).
3. The proposed flip is either accepted or not by comparing the acceptance ratio between S_1 and S_2 with a random number, $n \in [0 : 1]$, such that if $A(S_1 \rightarrow S_2) \geq n$ the flip is accepted.

4. If the flip has been accepted, the number of lipids in each lipid state is updated along with the system enthalpy.

This scheme is referred to as one Monte Carlo step. In the present implementation, selection of which lipid is proposed flipped is chosen at random. The standard “time” scale in Monte Carlo simulations is referred to as Monte Carlo cycles, and is defined as one Monte Carlo step per site (lipid) in the system.

When implementing the Monte Carlo simulation care has to be taken especially in the transition region in regard to equilibration of the simulation and also with finite size effects due to the neighboring interactions of the Doniach model (see appendix: [Equilibration \(E.2\)](#) and [Finite Size Effects \(E.3\)](#) for details).

4.1.4 Simulation of the Doniach Model

The simulation efforts of the present thesis are all based on the Doniach model and explored using the Monte Carlo method with the Glauber algorithm. The model parameters used⁷ are the following [76]:

ΔH	36400 J/mol
ΔS	115.9 J/mol · K
ω_{fg}	1326.0 J/mol
T_m	314.05 K

All simulations have been carried out on a 100 by 100 hexagonal grid with periodic boundaries. To ensure that the region of state space sampled is the most likely, all simulations have equilibrated a minimum of 30 correlation times before sampling, effectively meaning more than $6 \cdot 10^4$ Monte Carlo cycles at the transition temperature.

In the simulations the system variables available are the system enthalpy and the fluid fraction. The excess heat capacities can be calculated from the simulated fluctuations of system enthalpy as described in [Susceptibilities](#) (appendix A.1). The associated error of the estimated heat capacity is estimated using the [Jackknife Method](#) (appendix E.4.2). The error of the fluid fraction can be calculated by the standard deviation (see Eq. (E.8)). All simulations of the heat capacity have been performed using an [Adoptive Algorithm](#) (appendix E.5). The applied adoptive algorithm ensures that sampling is of only strictly statistically independent measuring points.

⁷The noted transition temperature may differ slightly from the standard T_m for DPPC LUV in the literature. The difference is due to the precision of the chosen simulation parameters and holds no physical significance.

The excess heat capacity and the fluid fraction estimated from simulations of the lipid (DPPC) melting transition using the Doniach model is shown in Fig. (4.1).

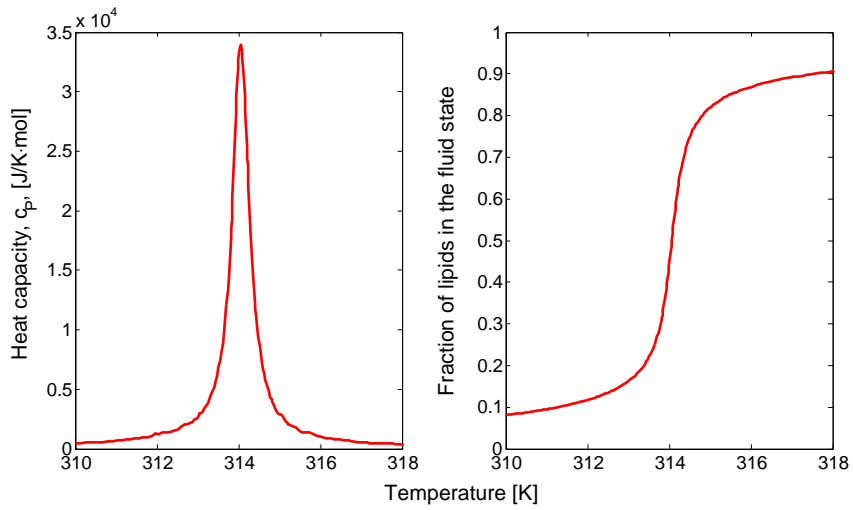


Figure 4.1: *Left:* Excess heat capacity found using Monte Carlo simulation of the Doniach model. *Right:* Fraction of lipids in the fluid state found again by Monte Carlo simulation of the Doniach model. Error bars have in both plots been omitted for clarity. The presented curves are spline fits of the raw data, where the inverse of the estimated errors have been used as weighting.

From the fluid fraction – area, density and background isothermal compressibility can be calculated using respectively, the known area per lipid (*gel*: 47.4 \AA^2 , *fluid*: 62.9 \AA^2), the known specific area (*gel*: $1.90 \cdot 10^6 \text{ cm}^2/g$, *fluid*: $2.52 \cdot 10^6 \text{ cm}^2/g$) and the known compressibility (*gel*: $1.0 \text{ m}/N$, *fluid*: $6.9 \text{ m}/N$) [39]. The isothermal compressibility can be calculated from the background compressibility, $\kappa_T^A(\infty)$, and the transition associated compressibility (Eq. (2.5)). The isothermal compressibility and the lateral density is shown in Fig. (4.2).

From Fig. (4.1) and Fig. (4.2) the lipid melting transition is not discontinuous, classifying the transition as weak first order, as noted in [Membrane Phase Transition](#).

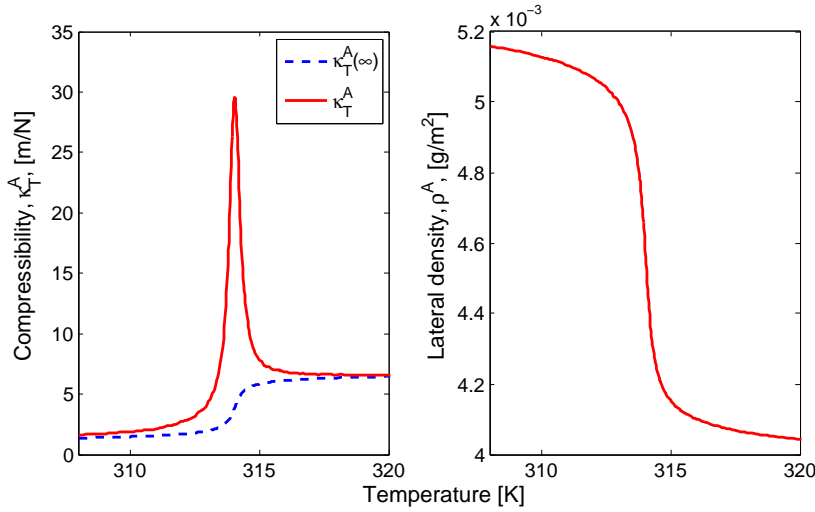


Figure 4.2: *Left:* Isothermal compressibility calculated from the fluid fraction and the excess heat capacity. *Right:* The lateral density calculated from the fluid fraction. Error bars have in both plots been omitted for clarity.

4.2 Relaxation Simulations

The main goal of this project is to map how lateral sound of different frequencies propagates through a lipid bilayer. For this, as discussed in [Adiabatic Pressure Perturbation](#) (section 3.1), the relaxation function of the dynamic heat capacity is needed. The goal of the relaxation simulations is to further justify the functional form of the relaxation function of the enthalpy but also to illustrate the response of the system to periodic pressure perturbations.

The relaxation function of a specific thermodynamical variable is a generic property of the system and is therefore independent, in its form, of the nature of the external parameters of the system, adiabatic or isothermal [89]. For conveniences the relaxation function will be studied in an isothermal system, since isothermal models of the lipid membrane are readily available. The example used here is the Doniach model.

Through the fluctuation-dissipation theorem⁸ the kinetics of a thermodynamical system can be probed by two very different approaches [90]. One being studying the fluctuations of a thermodynamical variable, the other being perturbing the system and studying the relaxation behavior of the system.

⁸The fluctuation-dissipation theorem states that the response of a system in equilibrium to a small perturbation is the same as the system's response to spontaneous fluctuations.

4.2.1 Fluctuation Simulations

The relaxation behavior of the enthalpy is of central importance for the analytical derivations. The goal of the fluctuation simulations is to verify the simulation findings by Grabitz *et al.* [18]. This covers both the verification of the single exponential relaxation behavior in the lipid melting transition and verification of the proportionality relation between the relaxation time and the heat capacity.

As ensured by the fluctuation-dissipation theorem, the time scale of the fluctuation (noise) around the equilibrium of a system describes the relaxation dynamics. The characteristic timescale of the enthalpy noise can be obtained using the autocorrelation function

$$G(t') = \frac{\int_0^\infty (H(t) - \langle H \rangle) \cdot (H(t + t') - \langle H \rangle) dt}{\int_0^\infty (H(t) - \langle H \rangle)^2 dt}, \quad (4.6)$$

where t' is the time lag. The function is normalized such that the function takes values between 1 at $t' = 0$ and 0 when t' approaches ∞ .

Fluctuation Results

The presented data from the fluctuation simulations is the average of at least 10 independent simulations, each sampled over a minimum of 10^5 Monte Carlo cycles where at each Monte Carlo cycle the system's enthalpy is printed. The autocorrelation function has been calculated using MATLAB's built-in `autocorr` function.

From Fig. (4.3) the single exponential relaxation behavior of the lipid (DPPC) melting phase transition is verified. The distortion of the linear slope of the *right* plots in Fig. (4.3) is due to the finale size of the sampled data sets, and should be considered as statistical noise. The autocorrelation functions of the enthalpy fluctuations have been fitted using MATLAB to single exponentials (Eq. (3.12))⁹. The relaxation times found by the fluctuation simulations have been plotted along with the simulated heat capacity in Fig. (4.4). For this, the found relaxation times in the transition region are well approximated as being proportional to the excess heat capacity.

From these results the single exponential relaxation behavior of the lipid membrane in the transition region is confirmed. Further, the proportionality relation between the excess heat capacity and the relaxation times from [18] has been reproduced.

⁹All presented fits has R-squared values above 0.9

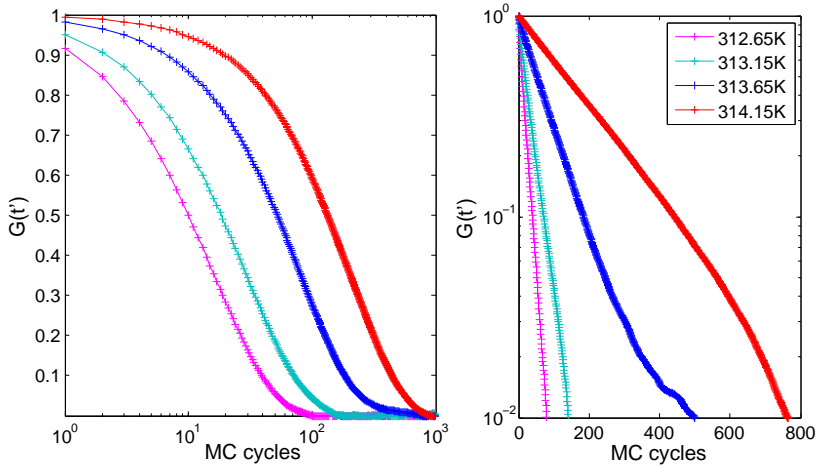


Figure 4.3: The autocorrelation function of fluctuations of the system enthalpy. *Left:* Shows the time scale of the fluctuations of system enthalpy. *Right:* Shows that the relaxation behavior of the fluctuations of the system enthalpy is well approximated by a single exponential. The presented data is representative for both below, in and above the transition temperature.

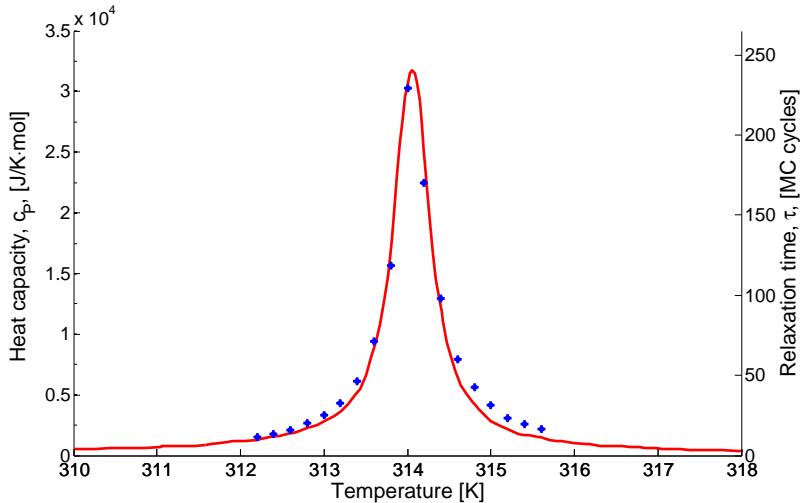


Figure 4.4: The relaxation times in the lipid (DPPC) melting transition compared to the functional form of the excess heat capacity. The *solid line* is the excess heat capacity found by Monte Carlo simulation of the Doniach model. The presented curve is a spline fit of the simulated data using the inverse of the estimated error as weighting. The *crosses* are the relaxation times of the equilibrium fluctuation, found by fitting the autocorrelation function with a single exponential.

4.2.2 Perturbation Simulations

The experimental methods available for probing the dynamics of a system through perturbations can be divided into *transient* and *stationary* perturbation methods [17]. Transient perturbation methods include temperature and pressure jump techniques as well as linear heating. The basic concept of this group of techniques is to make a small fast perturbation, moving the system out of equilibrium and probe the relaxation back to the new equilibrium state of the system. Small perturbations means that the system responds linearly to the perturbation. By fast perturbations is meant that the perturbation has to happen on timescales much faster than the relaxation process under investigation, such that important relaxation kinetics do not happen during the perturbation. The stationary perturbation method was introduced by Eigen in 1954 [67] with which he revolutionized kinetic probing techniques¹⁰. In stationary perturbation methods the system under investigation is perturbed in a periodic manner by small perturbations. The main advantage of these methods is that the requirement of the perturbations to be fast is circumvented and that averaging over time during sampling is possible – resulting in good noise to signal ratios. The finite relaxation rates in a system will, much like in sound propagation (dispersion and attenuation), result in a lag in the response of the system, taking the form of phase shift, and a lowering of the response amplitude.

The assumption of linear response of the system in thermodynamical equilibrium to small perturbations has been applied experimentally to the main transition of membranes with great success [17, 18]. There are formally two requirements for applying perturbation methods to study the kinetics of a phase transition [17]: The applied perturbation has to be of a variable that can change the “extent” of the phase transition and that the extent of the transition can be monitored through another variable. The requirement of an observable variable is easily met in a model system since all variables of the system are readily available. For the perturbation variable, the simplicity of the Doniach model means that any variable¹¹ that can change the enthalpy associated state change, ΔH , can be used. It is well known that the area of the lipids in the bilayer increases by about 25% from the gel to the fluid phase. The lateral pressure, Π , can therefore be used to apply the perturbation. The lateral pressure is related to the enthalpy by:

$$dH = TdS + VdP + Ad\Pi + \dots \quad (4.7)$$

¹⁰This discovery led to him receiving the 1967 Nobel prize in chemistry. See www.nobleprize.org

¹¹Choosing an intensive variable has the preferable advantage of being independent of system size.

From this, a perturbation of the lateral pressure will result in a change in the enthalpy change associated to a flip of the lipid state.

$$\Delta H = \Delta H_0 + \Delta A \cdot \delta \Pi, \quad (4.8)$$

where ΔH_0 is the known enthalpy change associated with the change of lipid state, containing all the non-perturbed contributions. $\delta \Pi$ is the change in lateral pressure from its physiological value. For the periodic perturbation a simple sinus with an adjustable amplitude, a_Π , has been chosen to simplify analyzing the response of the system ($\delta \Pi = a_\Pi \sin(\omega t)$). The size and the nature of the amplitude is not important for this thesis as long as the assumption of linear response of the system holds. The final form of the perturbed change in enthalpy is

$$\Delta H = \Delta H_0 + \Delta A \cdot a_\Pi \sin(\omega t), \quad (4.9)$$

where ω is the angular frequency of the perturbation and t is time. The area change between the two lipid states is $\Delta A = 15.5 \text{ \AA}^2$ [39].

Eq. (4.9) can be inserted directly into the Doniach model providing a simple perturbation extension of the model for probing the dynamics of the system. Note, that by changing the lateral pressure, the enthalpy contributions from all lipids in the fluid state change by:

$$\Delta H_{fluid} = \Delta A \cdot a_\Pi \sin(\omega t) \quad (4.10)$$

For Monte Carlo simulations of non-equilibrium experiments the dynamics of the model have to be chosen with care, since not only the end distribution of states is important, but also the way in which it is achieved [86]. Due to the equilibrium nature of the chosen simulation method (Monte Carlo) the lateral pressure perturbation is applied over the full system, such that there is no propagation dynamics needed. The only dynamics needed in simulations of a pure lipid system are the dynamics of the change in states of the lipids, since all lipids in the system are indistinguishable and movement of individual lipids therefore can not be tracked. Using the present implementation (simulation) as a near-equilibrium simulation is justified by the previous success in mimicking the relaxation behavior of the equilibrium fluctuations in the lipid melting transition [18].

Perturbation Results

Here the simulation results of the perturbation simulations will presented and discussed.

The implementation of the perturbation model extension of the Doniach model is done using Eq. (4.9) as the change in enthalpy for a lipid state change in Eq. (4.2) and keeping track of changes in enthalpy of lipids in the fluid state in accordance with Eq. (4.10).

Equilibration is in the perturbation simulations done first without the perturbation extension, and then again with the perturbations extension. The first equilibration is done to ensure that the region of state space explored during the perturbation simulations is close to the equilibrium region.

The raw simulation output with the applied perturbation is shown in Fig. (4.5).

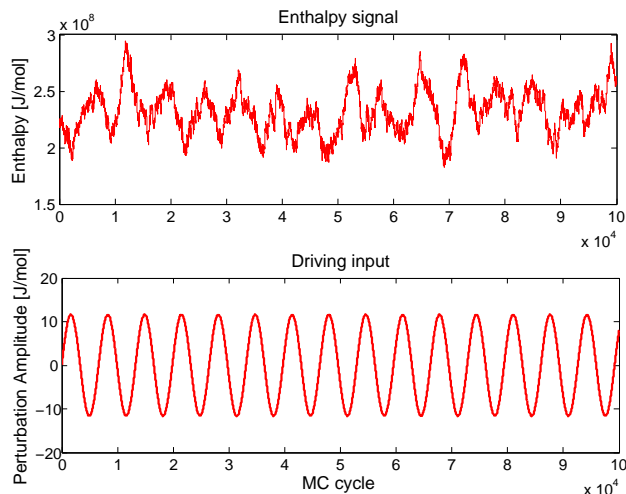


Figure 4.5: Raw simulation system enthalpy output with the applied perturbation. *Top:* The raw enthalpy signal at $T = 314.15 \text{ K} \approx T_m$. *Bottom:* The applied enthalpy perturbation, originating from the applied lateral pressure perturbation with $\omega = 1000 \text{ 1/(MC cycles)}$ and an amplitude of $a_{\Pi} = 0.75 \text{ N/m}$.

As clearly illustrated by Fig. (4.5), the simulated system enthalpy follows the applied perturbation with a phase shift. Along with that phase shift, the response amplitude of the system to the perturbation is also frequency and state dependent. In the phase transition the lipid membrane becomes very soft causing the response of the system to become very strong. This is modeled in the perturbation simulations by the free energy gain of flipping a lipid state being small in the transition – making the perturbation dominant.

For the purpose of exploring the relaxation behavior using periodic perturbation, the amplitude of the applied perturbation has to be small, meaning that the response of the system is a linear function of the perturbation. In Fig. (4.6) the square of the response has been fitted to a second order polynomial, verifying the linear response of amplitude in the explored range.

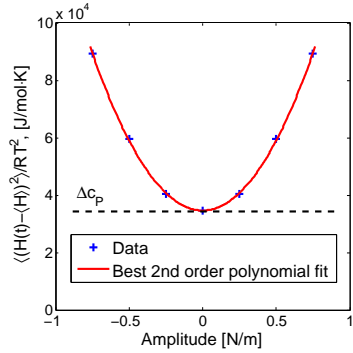


Figure 4.6: Amplitude of the system response as a function of the applied perturbation amplitude at $T = 314.15\text{ K} \approx T_m$. The presented simulated responses have been mirrored around zero perturbation.

Using that the model lipid membrane system responds in a linear fashion to lateral pressure perturbations, [Linear Response Theory](#) (appendix D) can be applied. From the chosen lateral pressure perturbation (Eq. (4.9)) the enthalpy response of the modeled lipid membrane takes the form

$$H(t) - \langle H \rangle = \text{Im} \left(\frac{a_H \exp(i(\omega t - \theta))}{(1 + (\omega\tau)^2)^{1/2}} \right) = \frac{a_H \sin(\omega t - \theta)}{(1 + (\omega\tau)^2)^{1/2}} \quad (4.11)$$

where

$$\tan(\theta) = \omega\tau. \quad (4.12)$$

In Eq. (4.11) and Eq. (4.12), θ is the phase shift between perturbation and response, ω is the angular frequency of the applied perturbation, a_H is the amplitude of the perturbation and τ is the lipid membrane's relaxation time. All perturbation simulations have been carried out with a perturbation amplitude of $a_{\Pi} = 0.75\text{ N/m}$, which according to Fig. (4.6) is well within the linear regime.

By cross-correlating the applied perturbation with system enthalpy, using MATLABs built-in `xcorr` function, and fitting this with $\sin(\omega t + \theta')$ ¹², the simulated phase shift can be estimated, see Fig. (4.7).

¹²The cross-correlation between $\sin(\omega t)$ and $\sin(\omega t + \theta)$ has the form $\cos(\omega t + \theta)$. When fitting to $\sin(\omega t + \theta')$, there will be a discrepancy between the two phase shifts of $\theta = \theta' - 2\pi + \pi/2$, where the 2π depends on the fitting procedure.

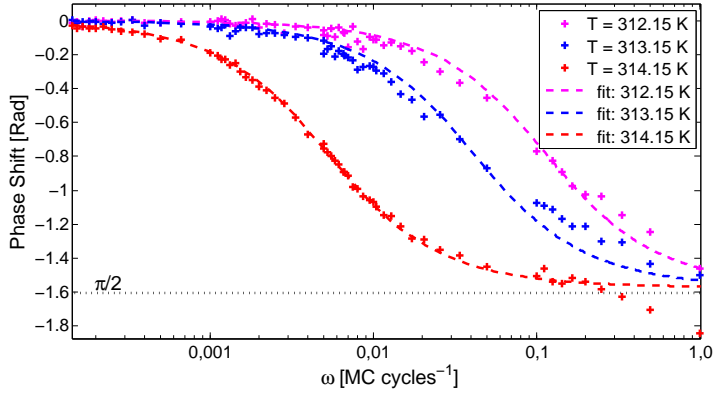


Figure 4.7: The phase shift between the applied lateral pressure perturbation and the enthalpy response of the system. The *crosses* are the estimated phase shifts at different frequency perturbations. The estimated phase shift has been fitted to Eq. (4.12) indicated by the *dotted line*. From the fits the corresponding relaxation times have been estimated: $\tau(312.15 \text{ K}) = 8.7 \pm 0.5 \text{ MC cycles}$, $\tau(314.15 \text{ K}) = 24.2 \pm 2.0 \text{ MC cycles}$ and $\tau(314.15 \text{ K}) = 188.5 \pm 7.2 \text{ MC cycles}$. The presented phase shifts are representative of the behavior in the full range of the transition.

The reader might notice that phase shifts are estimated down to $\omega = 1/(MC \text{ cycles})$, meaning that a full period of the perturbation is done during one Monte Carlo cycle. These “too low” frequency perturbations are achieved by not letting the simulation go through a full Monte Carlo cycle before printing the system enthalpy. In the low frequency perturbation simulation the enthalpy is printed 100 times during a single Monte Carlo cycle. This does not change the dynamics of the system, but going further down in frequency can result in effects of the course grain nature of the Doniach model to become apparent. The large noise on the low frequency phase lag estimates is due to very low signal to noise ratio, which is indirectly illustrated in Fig. (4.8).

In Eq. (4.11) the fluctuations of the system enthalpy have not been considered – fluctuations that, in the transition region, is very high. It is not possible directly from the enthalpy fluctuations to separate the perturbation response from spontaneous fluctuations. It is therefore a much more prudent approach to consider the average of the squared enthalpy fluctuation. Recognizing the analogy to the excess heat capacity, the spontaneous fluctuation component of the signal can easily be identified.

$$\frac{\langle (H(t) - \langle H \rangle)^2 \rangle}{RT^2} = \frac{a_H^2 / (2RT^2)}{1 + (\omega\tau)^2} + \Delta_{CP}, \quad (4.13)$$

where the first term is the response component and the second is the spon-

taneous fluctuation component (the equilibrium excess heat capacity).

In actually sampling the average of the squared enthalpy fluctuation it is important to make the averaging such that the periodic nature of the perturbation is accommodated. This has been done by sampling over one perturbation period and then average over the number of periods completed during the simulation. The number of periods sampled over in the simulation is the numerical value of $\langle (H(t) - \langle H \rangle)^2 \rangle / RT^2$ ¹³, hereby taking somewhat care of the diversity of the relaxation times in the transition. The nature of sampling, however, makes direct estimate of the error impossible. The noise of the presented data (see Fig. (4.8)) gives some measure of the error though.

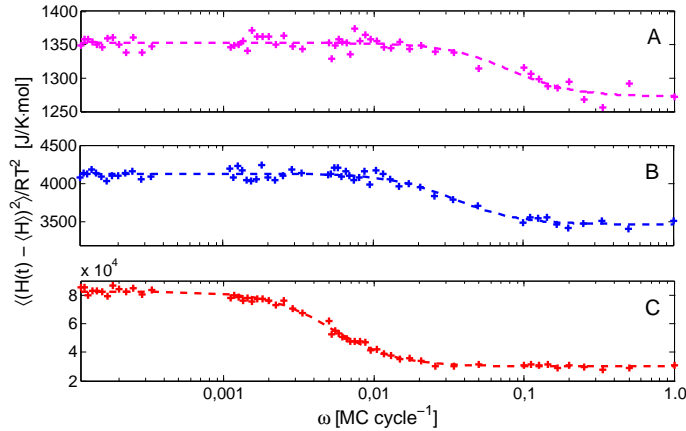


Figure 4.8: The amplitude of the lipid membrane response to lateral pressure perturbation of different frequencies. The *crosses* are the estimated amplitude at different frequency perturbations. The estimated amplitude has been fitted to Eq. (4.13), indicated by the *dotted line*. *A*: has been carried out at $T = 312.15\text{ K}$. *B*: $T = 313.15\text{ K}$. *C*: $T = 314.15\text{ K} \approx T_m$. The presented forms of the response amplitude are representative of the behavior in the full range of the transition.

By fitting the simulated amplitude of the lipid membrane response to Eq. (4.13), the relaxation time and the corresponding excess heat capacity is estimated:

T	τ	Δc_P
312.15 K	$12.6 \pm 4.2\text{ MC cycles}$	$1272 \pm 10\text{ J/mol}\cdot\text{K}$
313.15 K	$29.0 \pm 4.4\text{ MC cycles}$	$3471 \pm 40\text{ J/mol}\cdot\text{K}$
314.15 K	$190.6 \pm 10.1\text{ MC cycles}$	$30120 \pm 1040\text{ J/mol}\cdot\text{K}$

These values agree with the relaxation time found from the phase shift (see

¹³If $\langle (H(t) - \langle H \rangle)^2 \rangle / RT^2 = 9 \cdot 10^4$ than the number for periods sampled over is $9 \cdot 10^4$

Fig. (4.7)), as well as the ones found from the fluctuation simulations (see Fig. (4.4)). Further, the estimated excess heat capacities agree well with the values found from equilibrium simulations (see Fig. (4.1), *left*). These agreements holds throughout the extent of the transition.

The perturbation extension of the Doniach model has been shown to estimate both the relaxation time and the equilibrium excess capacity in agreement with the values obtained from equilibrium simulations of the Doniach model. This implies that the Doniach model can fairly easily be used as the basis for dynamical near-equilibrium simulations, which could prove useful as comparison to experiments probing dynamical properties of lipid membranes.

The perturbation simulations serves, in this thesis, to further illustrate the relaxation behavior of the lipid (DPPC) membrane in its melting transition. It also serves as an excellent illustration of how a system responds to sinusoidal perturbations in the linear regime, which is the basic nature of the response of the lipid membrane to sound. In this comparison it is, however, important to remember that sound is adiabatic in nature, whereas the perturbation simulations are of an isothermal system.

4.3 Finite System Simulations

The goal of the simulation efforts in this section is to relate the dynamic heat capacity to the adiabatic lateral compressibility. As proposed in [Adiabatic Compressibility](#) (section 3.2), the frequency dependence of the adiabatic compressibility is related to the frequency dependence of the lipid membrane's associated heat reservoir size. This concept has been used to successfully predict the limiting cases of no associated reservoir and an infinite reservoir [3]. The goal of the following proposed model is to connect these two limiting cases by exploring how a finite heat reservoir affects the thermodynamical properties of a lipid membrane. By finite heat reservoir is meant that the lipid membrane and its finite heat reservoir are *adiabatically isolated* from the exterior.

4.3.1 Adiabatic Model Extension

In an adiabatically isolated system enthalpy is strictly conserved, and any enthalpy supplied or absorbed by the lipid membrane in the process of lipid state fluctuations, needs to come from the surrounding system. Consequently, the thermodynamical system surrounding the lipid membrane will be considered as a energy reservoir (or buffer). In the Doniach model the membrane system is connected to an infinite water reservoir (Fig. (4.9), *left*), in effect keeping the temperature constant. In an infinite system conservation of enthalpy can be disregarded, since the enthalpy associated with a lipid state change is finite. This is, however, not the case for a finite system (Fig. (4.9), *right*), where much care has to be made in conserving the enthalpy.

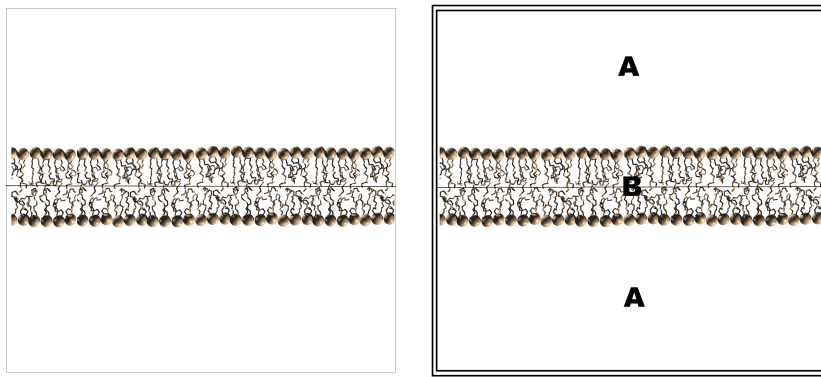


Figure 4.9: *Left:* A visualization of the system considered in the Doniach model. *Right:* The system considered in the present model extension. The double box surrounding the system indicates adiabatic isolation.

The thermodynamical system in consideration is: Two sub-ensembles, in which the number of particles and pressure are constant. These together, compose a unit ensemble that is isolated such that enthalpy (heat), number of particles, pressure and *temperature* are constant. This is illustrated in Fig. (4.10).

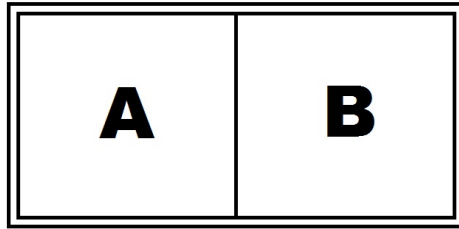


Figure 4.10: The thermodynamical system under consideration. The two sub-ensembles are denoted as *A* and *B*, and the adiabatic isolation is depicted by the double layered outer box.

Sub-ensemble *A* is the reservoir, which is comprised of the water surrounding the lipid membrane and the lipid chains which are assumed to be passive heat reservoirs of the lipids. The other sub-ensemble, *B*, is the lipid membrane, or rather a model (Donaich model) of the lipid membrane (illustrated in Fig. (4.9), *right*). The sub-ensembles are connected such that they can only exchange enthalpy between each other. The states that comprise the surrounding ensemble's state space are any superpositions of states of the two sub-ensembles that respect the constant enthalpy, pressure, number of particles and temperature of the total system. It is important to note that it is not the total system that is of interest, it is the sub-ensemble of the lipid membrane.

The probability of an internal enthalpy exchange between the sub-ensembles is the probability of one providing and the other absorbing. Using this analogy, the probability of a lipid state change in a finite adiabatic isolated system must be the probability of a lipid state change (flip) *and* the reservoir buffering (buff). Using the product rule this can be written as following:

$$p(\text{flip} \cap \text{buff}) = p(\text{flip})p(\text{buff}|\text{flip}), \quad (4.14)$$

where $p(\text{flip})$ is the probability of a given lipid state change and $p(\text{buff}|\text{flip})$ is the probability of the reservoir being able to buffer that change. Note, that in the case of an infinite reservoir $p(\text{buff}|\text{flip})$ will be 1, and $p(\text{flip} \cap \text{buff}) = p(\text{flip})$. In general, however, for a finite reservoir $p(\text{buff}|\text{flip}) < 1$, since the enthalpy available in the reservoir is finite.

The probability of a lipid state change

The probability of a lipid state change, $p(\text{flip})$, is independent of the system surrounding the membrane, and is known from the implementation of the Doniach model. The acceptance ratio¹⁴ of a lipid state change is, using Glauber algorithm, given by Eq. (4.5):

$$A(\text{flip}) = \frac{K}{K + 1}, \quad (4.15)$$

where

$$K = \exp \left(\frac{-\Delta G}{RT} \right). \quad (4.16)$$

The Gibbs free energy associated to a lipid state change, ΔG , is known from the Doniach model, Eq. (4.2).

The probability of the reservoir buffering a lipid state change

The probability (or rate) by which the reservoir is able to accommodate a specific need (absorb or supply) should be equal to the probability of the reservoir having a fluctuation that can accommodate the enthalpy change associated with a lipid state change. The probability of the reservoir having a fluctuation that can accommodate a given lipid state change can be calculated from the change in Gibbs free energy, ΔG_r , associated to such a fluctuation.

$$\Delta G_r = \Delta H_r - T\Delta S_r, \quad (4.17)$$

where ΔH_r is the change in enthalpy the reservoir needs to buffer for a proposed lipid state change¹⁵, ΔS_r is entropy change in the reservoir associated with the buffering of the enthalpy and T is the temperature of the total system.

The change in the reservoirs enthalpy from a given lipid state change is known since all changes in the lipid membrane's enthalpy have to be accommodated by the reservoir. The only unknown in Eq. (4.17) is the entropy change of the reservoir associated with the buffering of the enthalpy.

The fluctuation of the reservoir that can accommodate a given lipid state change can be of any thermodynamical variable, even the globally fixed, since the fluctuations are only in the reservoir sub-ensemble (local). In the following the reservoir temperature will be used as the fluctuating variable. It is important to emphasize that the temperature fluctuations only serve

¹⁴Remembering the relation between the transition probability and the acceptance ratio, Eq. (4.4).

¹⁵The enthalpy change associated with the change of a lipids state also encompass the changes in neighbor interactions.

as an enthalpy buffer for the lipid membrane. From the local fluctuations of temperature, the change in the reservoirs entropy associated with the transfer of enthalpy internally between the two sub-ensembles can be calculated as follows:

$$\left(\frac{\partial S}{\partial T}\right)_P = \frac{c_P}{T} \Rightarrow \quad (4.18)$$

$$\Delta S = \int_{T_1}^{T_2} \frac{c_P}{T} dT. \quad (4.19)$$

In the temperature range of interest ($T_m \pm 5$), the heat capacity of water can be assumed constant. Assuming likewise that the heat capacity of the lipid chains are constant¹⁶, the entropy change of the reservoir takes the form:

$$\Delta S_r = c_{P,r} \ln \frac{T_2}{T_1}, \quad (4.20)$$

where T_2 is the temperature of the reservoir needed to accommodate the change, which is given by:

$$c_p = \left(\frac{\partial H}{\partial T}\right)_P \Rightarrow \quad (4.21)$$

$$T_2 = \frac{\Delta H_r}{c_{P,r}} + T_1, \quad (4.22)$$

and T_1 is the present temperature of the reservoir. $c_{P,r}$ is the total heat capacity of the reservoir, i.e. the heat capacity of both the lipid chains and the water in the reservoir.

From Eq. (4.20), Eq. (4.17) can be written as,

$$\Delta G_r = \Delta H_r - T c_{P,r} \ln \frac{T_2}{T_1} = \Delta H_r - T c_{P,r} \ln \left(\frac{\frac{\Delta H_r}{c_{P,r}} + T_1}{T_1} \right), \quad (4.23)$$

where T is the temperature of the total system, which is also the mean temperature experienced by the reservoir.

From Eq. (4.23), the acceptance ratio of the reservoir being able to accommodate a given state change is, using the Glauber algorithm, given by:

$$A(\text{buff|flip}) = \frac{K'}{K' + 1}, \quad (4.24)$$

where

$$K' = \exp \left(\frac{-\Delta G_r}{RT} \right). \quad (4.25)$$

¹⁶The heat capacity of the lipid chains (DPPC) changes from 1600 $J/mol \cdot K$ for gel state to 1650 $J/mol \cdot K$ for the fluid state [91], but it will here be assumed constant.

The probability of a lipid state change in a finite water reservoir

From Eq. (4.15) and Eq. (4.25) the probability of a lipid state change in a finite adiabatic isolated system can be found in accordance with Eq. (4.14). The corresponding acceptance ratio is given by

$$A(\text{flip} \cap \text{buff}) = A(\text{flip})A(\text{buff}|\text{flip}) \quad (4.26)$$

$$= \frac{K}{K+1} \frac{K'}{K'+1}. \quad (4.27)$$

If the simulation decides to allow a change of state, the enthalpy associated with this change is absorbed or supplied by the reservoir. From this, T_1 is updated to the value of T_2 and hereby strictly conserves enthalpy.

This model extension is an equilibrium model and must therefore uphold detailed balance, this is shown in [Detailed Balance](#) (appendix E.1).

Model considerations

The motivation for making the model was to enable studying the lipid membrane in a finite water reservoir, specifically the lipid melting transition. The basic idea of the model is that the heat reservoir should accommodate any lipid state changes, hereby conserving enthalpy (heat) in the system.

The size of the heat reservoir have not been specified in the above. In the proposed model it is assumed that each lipid can interact with the full reservoir, meaning that the reservoir is completely shared. By assigning a finite reservoir per lipid, the size of the total reservoir will scale with the number of lipids. The enthalpy in the system likewise scales with the number of lipids. From this, the total heat reservoir experienced by the membrane is finite relative to its own size. Meaning that the properties of the adiabatic model extension are independent of the number of lipids in the system (see Fig. (4.11))¹⁷.

For simplicity, each lipid has been assigned a number of water molecules, specifically their heat capacity, along with the heat capacity of its lipid chains. The detailed thermodynamical coupling between water and the lipid membranes is not known and is still a topic of much investigation [34]. The water associated to the lipid membrane is therefore assumed to have the properties of water in bulk solution. The actual amount of water assigned to each lipid is no physical importance, only the heat capacity of the reservoir is important and not its origin.

¹⁷Though numerically, the size of the total reservoir can lead to issues with precision in simulations.

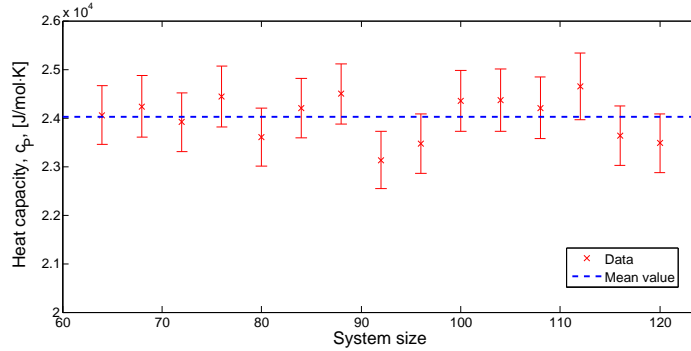


Figure 4.11: The excess heat capacity of the lipid membrane in a finite system of 1000 water molecules per lipid estimated for different system sizes. The number of lipids is the square of the system size.

The basic concept of the adiabatic model extension is that fluctuations in the heat reservoir can accommodate the lipid state changes. The detailed fluctuation of the heat reservoir is however not considered, only the probability of the reservoir having a fluctuation that can accommodate a given lipid state change is considered. In this, it is assumed that fluctuations in the heat reservoir are much faster than the characteristic rate of lipid state changes. This assumption is justified by both water¹⁸ and rotation of lipid chains [32] have characteristic timescales of the order ns , whereas the fastest relaxation times of the lipid membrane, during the lipid melting transition, are of the order of ms .

Note that the lipid membrane sub-ensemble experiences the temperature of the total system, which is constant, and has constant pressure. From this, the excess heat capacity of the lipid membrane can be calculated directly from its enthalpy fluctuations (see appendix A.1 for details on calculation).

¹⁸For a discussion on water, its structure and characteristic timescales, see the homepage of Martin Chaplin: www.lsbu.ac.uk/water/methods.html.

4.3.2 Results

In this section the simulation results of the adiabatic model extension will be presented, and the posed ansatz (Eq. (3.22)) is discussed in the light of these results.

The heat reservoir assigned per lipid in the simulations, are the heat capacity of a number of water molecules and one lipid chain pair. The heat capacities used is: $c_p^{water} = 74.539 \text{ J/(K} \cdot \text{mol})$ ($= 1 \text{ cal/(g} \cdot \text{K)}$) for water in bulk solution and $c_p^{chain} = 1600 \text{ J/(K} \cdot \text{mol})$ for the lipid chains (DPPC) (gel state) [91]. The total heat capacity of the heat reservoir (per lipid) is given by:

$$c_{P,r} = c_p^{water} \cdot N_{water} + c_p^{chain}, \quad (4.28)$$

where N_{water} is the number of water molecules assigned to each lipid.

The total heat reservoir is shared by all lipids in the lipid membrane, and the minimum number of water molecules per lipid considered in any simulation is 100. Based on this, it is safe to assume in all simulations that $\Delta H_r/c_{P,r} \ll T_1$. Using this Eq. (4.23) can be well approximated by

$$\Delta G_r \approx \Delta H_r \left(1 - \frac{T}{T_1} \right) \quad (4.29)$$

This approximation is used in the simulations to avoid the computation time cost associated with calculation of the logarithm in Eq. (4.23)¹⁹.

The adiabatic model extension have been implemented using the implementation scheme in [Implementation of the Simulation](#) (section 4.1.3), where the acceptance ratio is given by Eq. (4.27). Note however that the acceptance ratio, Eq. (4.27), has in the present implementation been multiplied²⁰ by 2. This is done to ensure that the characteristic time scale of the simulations of the adiabatic model extension are similar to that of the simulations of the Doniach model, such that the adoptive algorithm can be used.

All simulations have been conducted as presented in [Simulation of the Doniach Model](#) (section 4.1.4), with the exception that equilibration has been done first without the model extension, followed by a separate equilibration with the model extension.

¹⁹This approximation slightly obscure detailed balance but have been shown to only have a minor effect on the simulation results (a shift in the transition temperature of about 0.02 K).

²⁰Multiplying the acceptance ratio by a constant can always be done without violating detailed balance or ergodicity.

From the simulations the effect of having a finite heat reservoir is clear. By lowering the available heat reservoir the phase transition associated phenomena are lowered, illustrated by a lowering of the heat capacity with smaller reservoirs. This lowering is due to the hampering of large scale enthalpy fluctuations in the lipid membrane. The width of the phase transition is unaltered, meaning a depression of the phase transition with smaller heat reservoirs and not a out-smearing. This is illustrated in Fig. (4.12).

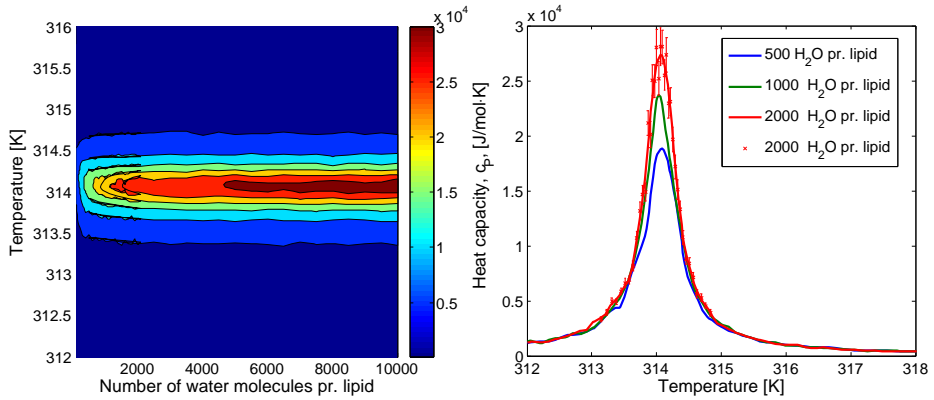


Figure 4.12: *Left:* A contour map of the heat capacity of the lipid membrane, where the coloring is done in accordance with the value of the heat capacity. *Right:* Heat capacity profiles of the lipid membrane for different sizes of associated heat reservoirs. The curves are obtained by spline fitting raw simulation data using the inverse estimated error as weighting. Error bars have been omitted for clarity in all plots but one. Due to the adoptive algorithm the error is the same relative to the heat capacity for all simulations.

In **Adiabatic Compressibility** (section 3.2) it was posed as an ansatz that the heat capacity, $c_P^{effective}$, of the lipid membrane in a adiabatically isolated heat reservoir has the form of Eq. (3.21):

$$c_P^{effective} = c_P^{ex} - \frac{(c_P^{ex})^2}{c_P^{system}}$$

where

$$c_P^{system}(\omega) = c_P^{ex} + c_{P,r}.$$

In the present model the heat capacity of the total heat reservoir, $c_{P,r}$, is an input parameter and the excess heat capacity of the lipid melting transition is known from Fig. (4.1). Using these, the effective heat capacity can be directly calculated and be compared with the simulation results, hereby testing the ansatz. For verification of the ansatz, the simulated estimates of the excess heat capacity for finite heat reservoirs are plotted in Fig. (4.13) along with the calculated effective heat capacity.

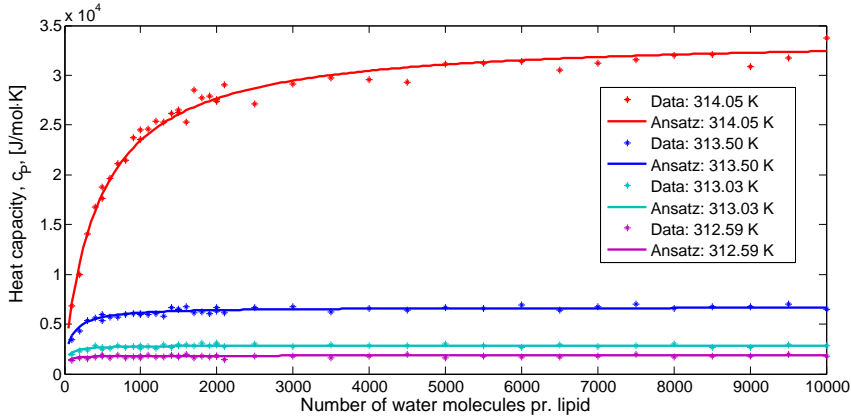


Figure 4.13: Verification of the posed ansatz. *full line*: The effective heat capacity calculated from Eq. (3.21) at different temperatures and for different reservoir sizes. *Crosses*: The simulated estimate of the excess heat capacity of the lipid membrane for finite heat reservoirs. These represent the general behavior over the full transition range.

The estimated heat capacities have been spline fitted using the inverse error as weighting. This procedure is conservative in estimating the top point of the heat capacity when the peak becomes shapes. Taking this into account, Fig. (4.13) shows almost perfect agreement between Eq. (3.21) and the simulated estimate of the heat capacity, hereby verifying the validity of the posed ansatz.

The ansatz made it possible to recognized the effective heat capacity of the lipid membrane in a finite water reservoir as the dynamical heat capacity. This link become apparent when comparing the lowering of the heat capacity in Fig. (4.12) with the experimental results of Van Osdol *et al.* [70] shown in Fig. (3.1).

That the lipid membrane can be considered as a pseudo 2-dimensional system embedded in a 3-dimensional system has complicated the step of relating the dynamic heat capacity to the adiabatic compressibility. By the simulations of the proposed model, it is possible to probe how the properties of the lipid membrane, in the transition region, act when the extent of the associated heat reservoir become finite. The model is based on simple assumptions regarding the nature on the internal transfer of heat and should be applicable to not only the lipid membrane system, but to all lower dimensional system submerge in higher dimensional system, where the internal transfer rates in the heat reservoir can be considered much faster than the subsystem-subsystem transfer rates.

Chapter 5

Discussion and Conclusion

In the general interest of understanding the dynamics of the lipid melting transition, a wide array of experimental methods have been utilized over the years, ranging from pressure jump experiment [18] to ultra-sonic experiments [16, 58]. All attempts to describe sound propagation in the lipid membrane have thus up until this thesis been aimed at probing the relaxation behavior in the ultra-sonic regime. With the introduction of the Soliton model, which describes nerve signals as localized sound packets, understanding sound propagation at low frequencies become important for our understanding of nerves signals.

The goal of this work has been to estimate the frequency dependence of the lateral speed of sound in lipid membranes, using both analytically and numerically tools. These efforts will here be discussed and conclusions will be drawn from the findings. Last, perspectives and the general impact of the present work will be considered.

5.1 Discussion

In this thesis an analytic expression for the speed of sound in the plane of a lipid membrane during the lipid melting transition has been derived. In order to reach this point there were two main challenges:

1. Estimating the response behavior of the lipid membrane to periodic adiabatic perturbations.
2. Relate this response of the system to the speed of lateral sound – through the adiabatic lateral compressibility.

The response of the lipid membrane to adiabatic periodic perturbations is strongly related to the relaxation behavior of the system [54,57]. Following the derivations of Van Osdol *et al.* [17] using thermodynamics and a linear

response approximation¹, it was possible to simplify the response of the lipid membrane to a single response function utilizing a single exponential relaxation function. The response function takes the form of a dynamic heat capacity, which can be conceptually be understood as the effective heat capacity of the lipid membrane subject to adiabatic periodic perturbations.

In these derivations the major assumption concerns the nature of the relaxation function. Grabitz *et al.* [18] found that, in the lipid melting transition, the relaxation behavior of the lipid membrane, at low frequencies, is well approximated by a single exponential. This means that the lipid melting transition is *not* critical, which is verified by the final extent of the excess heat capacity. The single exponential relaxation behavior should, however, only be considered as a low frequency approximation to the dynamics of the lipid membrane in the lipid melting transition. In a number of ultra-sonic experiments it has been shown that the single exponential relaxation behavior is insufficient to describe the dynamics of the cooperative processes of the lipid melting transition in the ultra-sonic regime [16, 58].

As a conservative estimate, the single exponential relaxation behavior and thereby the validity of the estimated speed of sound, is thus limited to frequencies of the order of magnitude similar to the relaxation rate or lower.

The challenge of relating the periodic adiabatic perturbation response of the lipid membrane to the speed of sound is geometric in nature. The lipid membrane can be considered a pseudo 2-dimensional system embedded in a 3-dimensional system (a heat reservoir). All existing theories in the literature regarding relating the dynamic heat capacity to the adiabatic compressibility is based on the assumption that the medium of interest spans the full thermodynamical system. Halstenberg *et al.* [69] proposed that the frequency dependency of the adiabatic lateral compressibility in the lipid melting transition, originates from the sizes of the membrane associated heat reservoir and not from internal dynamics in the lipid membrane.

Motivated by this concept, a model was here proposed to probe the effects of a finite heat reservoir (adiabatically isolated) on the lipid melting transition. The idea of the model is, that any enthalpy changes in the lipid membrane have be supported by the heat reservoir. As the size of the heat reservoir becomes finite, the probability of the reservoir supporting a proposed change is lowered, thus limiting the extent of the lipid melting transition. To the present author's knowledge this is the first model exploring how the lipid melting transition is effected by a finite water reservoir. The simulation results of the proposed model, showed that the frequency dependent part of the adiabatic lateral compressibility can be interpreted as the effective heat

¹The linear response approximation is with regard to the perturbation amplitude, where the amplitude is assumed to be small.

capacity of a lipid membrane in a finite adiabatically isolated heat reservoir. The frequency dependent part of the adiabatic lateral compressibility is thus directly related to the dynamic heat capacity. The link between the dynamic heat capacity and the adiabatic compressibility proposed here, should be considered an extension of the concept of Halstenberg *et al.* [69], but it is the first justification that the relation hold in general.

From the response function (the dynamic heat capacity) and the relation between the dynamic heat capacity and the adiabatic compressibility, an analytic expression for the speed of sound in the plane of a lipid membrane was formulated. From values of the well known lipid membrane system, vesicles of DPPC, the speed of sound was calculated and was found to be in perfect agreement with existing estimates of the high and low frequency limits [3]. Using the low frequency approximation used in the Soliton model for the dispersion, the “dispersion constant” was found to be of the order of 10^8 times larger (at transition temperature) than estimated by Heimburg and Jackson [3] ($h = 2 \text{ m}^4/\text{s}^2$), and strongly dependent on lateral density during the lipid melting transition. Heimburg and Jackson estimated their dispersion constant from the width of a nerve pulse, whereas the estimate here is based on the properties of the highly cooperative pure lipid system of DPPC. Realistic characteristic relaxation times for nerve membrane in the transition can be assumed to be of the order of 10^2 to 10^3 times slower than for pure lipid membranes of DPPC. Assuming this, the estimated dispersion term will be of the order $10^2 \text{ m}^4/\text{s}^2$ to $10^4 \text{ m}^4/\text{s}^2$ at the transition temperature and $10^{-4} \text{ m}^4/\text{s}^2$ to $10^{-2} \text{ m}^4/\text{s}^2$ at the boarder of the transition. Taking this into account along with the density dependency of the “dispersion constant”, the estimated dispersion seem realistic in regard to the Soliton model.

An interesting new discovery regarding the estimated dispersion constant is its dependency on the relaxation time. The analytic form of the dispersion constant, is some function of the correlation length of the system (which is direct related to the excess heat capacity) times the relaxation time squared. The fact that the relaxation time enters squared, is from the perspective of the origin of the dispersion rather intuitive. The mechanism that causes dispersion in the lipid melting transition is the finite value of the relaxation rate. The meaningful variable for dispersion is however not the relaxation time, but rather $\omega\tau$, which is also consensus in the ultra-sonic field. It is the finite value of $\omega\tau$ that causes dispersion. Based on this argument, any Taylor expansion of the phase velocity to any given order around $\omega = 0$, should give some prefactor and the relaxation time to that order. This prediction fits nicely with the Taylor expansion of the BF-theory [65]. Posed here as speculation, the dependency of the dispersion on the relaxation time must be a general property of dispersion of this nature independent on the specific system.

5.2 Conclusion and Perspectives

It was the goal of this thesis to estimate the frequency dependence of the speed of sound in the plane of lipid membranes, specifically understanding dispersion in a model membrane of DPPC at low frequencies.

This work is the first in the literature aimed at exploring the frequency dependence of the sound propagation in lipid membranes at low frequencies. The main achievement of this thesis has been to formulate a analytic expression for sound propagation in the lipid membrane based entirely on thermodynamics, using the concept known from the theory of sound propagation. In doing this a relation between the lipid membranes response to sound propagation and the speed of sound was formulated and justified by simulations, modeling how the lipid melting transition is affected by a finite heat reservoir.

For vesicles of DPPC, the frequency dependence of the speed of sound (dispersion) was found, to be very strong and also that the dispersion is strongly dependent on lateral density.

Perspectives

The major limitation of the present analytic expression for the speed of sound is its limitations in frequency range. It could in the future be interesting and useful to extend the applied dynamics to cover a broader frequency range unifying the experimental results in the low frequency regime with the results in the ultra-sonic regime. A possible approach to this, would be the theory proposed by Bhattacharjee and Ferrel [65] (BF-theory), which has been successfully applied to the lipid phase transition by Halstenberg *et al.* [58] in the ultrasonic regime.

In the future, an exploration of the generality of the found relation between the dynamic heat capacity and the adiabatic compressibility could extent the present understanding of sound propagation in mediums not spanning the full dimensions of a thermodynamical system.

For the application of the present framework on biological membranes, a great experimental task still lies ahead in probing the general thermodynamical and dynamic behavior of these complex structures.

In the future it will be interesting to explore the implication of the present work on the Soliton model. In the present form, the Soliton model assumes that dispersion is independent of density or lipid state and the functional form of the dispersion term can be viewed as the lowest, non-trivial, order

expansion of the speed of lateral sound. The work of this thesis has shown that the dispersion “constant” is strongly dependent on density and has made a number of prediction regarding the general nature of dispersion in lipid membranes. In the future it will be interesting to see the dispersion constant estimated here incorporated in the Soliton model, thus possibly lead to a reformulation of the dispersion term. This work will thus enhance the predictive power of the Soliton model, and have deep reaching consequences for how the propagation of nerve signals is understood.

Bibliography

- [1] Cell, Invitrogen: <http://invitrogen.com>.
- [2] A. L. Hodgkin and A. F. Huxley, *The Journal of physiology* **117**, 500 (1952).
- [3] T. Heimburg and A. D. Jackson, *PNAS* **102**, 9790 (2005).
- [4] B. C. Abbott, A. V. Hill, and J. V. Howarth, *Proceedings of the Royal Society of London. Series B, Biological Sciences* **148**, 149 (1958).
- [5] J. M. Ritchie and R. D. Keynes, *Quart. rev. of biophysics* **18**, 451 (1985).
- [6] I. Tasaki, K. Kusano, and P. M. Byrne, *Biophysical journal* **55**, 1033 (1989).
- [7] I. Tasaki and P. Byrne, *The Japanese Journal of Physiology* **42**, 805 (1992).
- [8] T. Heimburg and A. D. Jackson, *Biophysical Reviews and Letters* **2**, 57 (2007).
- [9] S. S. L. Andersen, A. D. Jackson, and T. Heimburg, *Progress in neurobiology* **88**, 104 (2009).
- [10] D. L. Melchior, H. J. Morowitz, J. M. Sturtevant, and T. Y. Tsong, *Biochimica et biophysica acta* **219**, 114 (1970).
- [11] T. Heimburg, *Thermal biophysics of membranes* (Wiley-VHC, 2007).
- [12] J. R. Hazel, *American Journal of Physiology* **236**, R91 (1979).
- [13] E. F. DeLong and A. A. Yayanos, *Science* **228**, 1101 (1985).
- [14] T. Y. Tsong, T. T. Tsong, E. Kingsley, and R. Siliciano, *Biophysical journal* **16**, 1091 (1976).
- [15] T. Y. Tsong and M. I. Kanehisa, *Biochemistry* **16**, 2674 (1977).

- [16] S. Mitaku and T. Date, *Biochimica et biophysica acta* **688**, 411 (1982).
- [17] W. W. Van Osdol and R. L. Biltonen, *Journal of Biochemical and* **20**, 1 (1989).
- [18] P. Grabitz, V. P. Ivanova, and T. Heimburg, *Biophysical journal* **82**, 299 (2002).
- [19] E. Overton, *Vierteljahrsschrift der Naturforschende Gessellschaft (Zürich)* **44**, 88 (1899).
- [20] E. M. D. Gorter and F. Grendel, *Journal of Experimental Medicine* **41**, 439 (1925).
- [21] J. F. Danielli and E. N. Harvey, *Journal of Cellular and Comparative Physiology* **5**, 483 (1935).
- [22] S. J. Singer and G. L. Nicolson, *Science (New York, N.Y.)* **175**, 720 (1972).
- [23] O. G. Mouritsen and M. Bloom, *Biophysical journal* **46**, 141 (1984).
- [24] M. Eisenberg and S. McLaughlin, *BioScience* **26**, 436 (1976).
- [25] T. Heimburg and A. D. Jackson, *Thermodynamics of the nervous impulse*, in *Structure and dynamics of membranous interfaces*, chap. 12, pp. 318–335, John Wiley and Sons, Inc, 2008.
- [26] D. Marsh, *Chemistry and physics of lipids* **57**, 109 (1991).
- [27] M. Janiak, D. Small, and G. Shipley, *Journal of Biological Chemistry* **254**, 6068 (1979).
- [28] T. Heimburg, *Biophysical journal* **78**, 1154 (2000).
- [29] J. F. Nagle, *Annual Review of Physical Chemistry* **31**, 157 (1980).
- [30] G. Cevc, *Chemistry and physics of lipids* **57**, 293 (1991).
- [31] M. Fidorra, *Untersuchung des phasenverhaltens von membranen durch konfokale mikroskopie und kalorimetrie*, 2004.
- [32] W. Schrader, S. Halstenberg, R. Behrends, and U. Kaatze, *The Journal of Physical Chemistry B* **107**, 14457 (2003).
- [33] H. Ebel, P. Grabitz, and T. Heimburg, *The Journal of Physical Chemistry B* **105**, 7353 (2001).
- [34] A. S. Ulrich, M. Sami, and A. Watts, *Biochimica et biophysica acta* **1191**, 225 (1994).

- [35] J. M. Sturtevant, Chemistry and Physics of Lipids **95**, 163 (1998).
- [36] W. W. van Osdol, Q. Ye, M. L. Johnson, and R. L. Biltonen, Biophysical journal **63**, 1011 (1992).
- [37] H. M. Seeger, M. L. Gudmundsson, and T. Heimburg, The journal of physical chemistry. B **111**, 13858 (2007).
- [38] B. Gruenewald, S. Stankowski, and A. Blume, FEBS letters **102**, 227 (1979).
- [39] T. Heimburg, Biochimica et biophysica acta **1415**, 147 (1998).
- [40] U. R. Pedersen, G. H. Peters, T. B. Schrøder, and J. C. Dyre, The Journal of Physical Chemistry B **114**, 2124 (2010).
- [41] D. Steppich *et al.*, Physical Review E **81**, 1 (2010).
- [42] S. Ochs, *A history of nerve functions* (Cambridge University Press, 2004).
- [43] K. S. Cole and H. J. Curtis, The Journal of general physiology **22**, 649 (1939).
- [44] Y. Kobatake, I. Tasaki, and A. Watanabe, Advances in Biophysics **2**, 1 (1971).
- [45] I. Tasaki, Ferroelectrics **220**, 305 (1999).
- [46] I. Tasaki, A. Watanabe, and I. Singer, PNAS **56**, 1116 (1966).
- [47] K. Iwasa, I. Tasaki, and R. C. Gibbons, Science **210**, 338 (1980).
- [48] K. Iwasa and I. Tasaki, Biochemical and biophysical research communications **95**, 1328 (1980).
- [49] P. M. Mendes *et al.*, Journal of Physical Chemistry B **110**, 3845 (2006).
- [50] B. Lautrup, A. D. Jackson, and T. Heimburg, ArXiv:physics/0510106v1 (2005), 0510106v1.
- [51] B. Lautrup, R. Appali, A. D. Jackson, and T. Heimburg, The European physical journal. E, Soft matter **34**, 1 (2011).
- [52] C. G. Stokes, Transactions of the Cambridge Philosophical Society **8**, 287 (1845).
- [53] G. Kirchhoff, Annalen der Physik **210**, 177 (1868).
- [54] K. F. Herzfeld and F. O. Rice, Physical Review **31**, 691 (1928).

- [55] M. Odonnell, E. T. Jaynes, and J. G. Miller, Acoustical Society of America, Journal **69**, 696 (1981).
- [56] M. Eigen and L. C. De Maeyer, Inverstigation of rates and mechanisms of reactions, in *Techniques in organic chemistry*, edited by A. Weissberger, pp. 896–1054, , 2nd ed., 1963.
- [57] M. Fixman, The Journal of Chemical Physics **36**, 310 (1962).
- [58] S. Halstenberg, W. Schrader, P. Das, J. K. Bhattacharjee, and U. Kaatze, The Journal of Chemical Physics **118**, 5683 (2003).
- [59] B. Brüning, E. Wald, W. Schrader, R. Behrends, and U. Kaatze, Soft Matter **5**, 3340 (2009).
- [60] K. Kawasaki, Physical Review A **1**, 1750 (1970).
- [61] D. M. Kroll and J. M. Ruhland, Physical Review A **23**, 371 (1981).
- [62] J. K. Bhattacharjee and R. A. Ferrell, Physical Review A **24**, 1643 (1981).
- [63] R. A. Ferrell and J. K. Bhattacharjee, Physical Review A **31**, 1788 (1985).
- [64] H. Tanaka, Y. Wada, and H. Nakajima, Chemical Physics **68**, 223 (1982).
- [65] J. K. Bhattacharjee and R. A. Ferrell, Physical Review E **56**, 5549 (1997).
- [66] L. Onsager, Physical Review **38**, 2265 (1931).
- [67] M. Eigen, Discussions of the Faraday Society **17**, 194 (1954).
- [68] A. H. Wilson, Thermodynamics and Statistical Mechanics, chap. 3, Cambridge University Press, , 1st ed., 1957.
- [69] S. Halstenberg, T. Heimburg, T. Hianik, U. Kaatze, and R. Krivanek, Biophysical journal **75**, 264 (1998).
- [70] W. W. Van Osdol, M. L. Johnson, Q. Ye, and R. L. Biltonen, Biophysical journal **59**, 775 (1991).
- [71] M. Barmatz and I. Rudnick, Physical Review **170** (1968).
- [72] A. B. Pippard, Philosophical Magazine **1**, 473 (1956).
- [73] M. J. Buckingham and W. M. Fairbank, *Progress in Low Temperature Physics* (North-Holland Publishing Co., Amsterdam, 1961).

- [74] W. Schrader *et al.*, The Journal of Physical Chemistry B **106**, 6581 (2002).
- [75] S. Mabrey, Proceedings of the National Academy of Sciences **73**, 3862 (1976).
- [76] V. P. Ivanova and T. Heimburg, Physical Review E **63**, 1914 (2001).
- [77] S. Doniach, The Journal of Chemical Physics **68**, 4912 (1978).
- [78] E. Ising, Zeitschrift für Physik A Hadrons and Nuclei **31**, 253 (1925).
- [79] D. A. Pink, T. J. Green, and D. Chapman, Biochemistry **19**, 349 (1980).
- [80] O. G. Mouritsen *et al.*, The Journal of Chemical Physics **79**, 2027 (1983).
- [81] I. P. Sugar, R. L. Biltonen, and N. Mitchard, Methods in enzymology **240**, 569 (1994).
- [82] S. Mabrey and J. M. Sturtevant, Biophysics **486**, 444 (1977).
- [83] A. J. Wagner, S. Loew, and S. May, Biophysical journal **93**, 4268 (2007).
- [84] V. P. Ivanova, I. M. Makarov, T. E. Schäffer, and T. Heimburg, Biophysical journal **84**, 2427 (2003).
- [85] A. Blicher, Permeability studies of lipid vesicles by Fluorescence Correlation Spectroscopy and Monte Carlo simulations, 2007.
- [86] M. E. J. Newman and G. T. Barkema, *Monte Carlo Methods in Statistical Physics*, 1st ed. (Oxford University Press, 1999).
- [87] N. Metropolis, A. W. Rosenbluth, M. N. Rosenbluth, A. H. Teller, and E. Teller, The journal of chemical physics **21**, 1087 (1953).
- [88] R. J. Glauber, Journal of Mathematical Physics **4**, 294 (1963).
- [89] H. B. Callen and R. F. Greene, Physical Review **86**, 702 (1952).
- [90] H. Nyquist, Physical Review **32**, 110 (1928).
- [91] A. Blume, Biochemistry **22**, 5436 (1983).
- [92] L. D. Landau and E. M. Lifshitz, *Fluid Mechanics*, Course of Theoretical Physics Vol. 6 (Pergamon Press, 1987).

Appendix A

Thermodynamics

This appendix section contains derivations of thermodynamical relations used in the course of the thesis.

A.1 Susceptibilities

At equilibrium the free variables of a system will fluctuate reversibly around their equilibrium value. From these fluctuations the susceptibilities of the system can be found, among these is the heat capacity. At constant pressure, the heat capacity, c_p , is defined as

$$c_P = \left(\frac{dQ}{dT} \right)_P. \quad (\text{A.1})$$

Enthalpy is defined as $H \equiv U + PV$. The differential is then $dH = dU + PdV + VdP$. By substituting in $dU = dQ - PdV$, dH will be reduced to $dH = dQ$, at constant pressure. From this Eq. (A.1) takes the form

$$c_P = \left(\frac{dH}{dT} \right)_P. \quad (\text{A.2})$$

¹ Using the statistical mechanical approach to thermodynamics, the thermodynamics variables can be considered as average values.

$$\langle H \rangle = \frac{\sum_i H_i \cdot e^{-H_i/RT}}{\sum_i e^{-H_i/RT}} = \frac{\sum_i H_i \cdot e^{-H_i/RT}}{Z}, \quad (\text{A.3})$$

¹Same procedure can be done for the entropy, since $dQ = TdS$, so $c_P = T \left(\frac{dS}{dT} \right)_P$.

where R is the gas constant, T is the temperature and Z is the partition sum. The sums are over all possible states of the system. Using Eq. (A.3),

$$\begin{aligned} c_p &= \left(\frac{d}{dT} \frac{\sum_i H_i \cdot e^{-H_i/RT}}{Z} \right)_p \\ &= \frac{\sum_i H_i^2 \cdot e^{-H_i/RT}}{RT^2 \cdot Z} - \frac{1}{RT^2} \frac{\sum_i H_i \cdot e^{-H_i/RT}}{Z} \frac{\sum_j H_j \cdot e^{-H_j/RT}}{Z} \\ &= \frac{\langle H^2 \rangle - \langle H \rangle^2}{RT^2}. \end{aligned} \quad (\text{A.4})$$

A similar derivation can be carried out for the isothermal lateral compressibility:

$$\begin{aligned} \kappa_T^A &= - \left(\frac{1}{\langle A \rangle} \cdot \frac{d \langle A \rangle}{d\Pi} \right)_T, \quad \langle A \rangle = \frac{\sum_i A_i \cdot e^{-H_i/RT}}{\sum_i e^{-H_i/RT}} \\ &= - \frac{1}{\langle A \rangle} \left(\frac{d}{d\Pi} \frac{\sum_i A_i \cdot e^{-H_i/RT}}{Z} \right)_T \\ &= \frac{\langle A^2 \rangle - \langle A \rangle^2}{\langle A \rangle RT}, \end{aligned} \quad (\text{A.5})$$

where Π is the lateral pressure which is related to the enthalpy through $H = U + pV + \Pi A$.

Using the proportionality relation, $\Delta A = \gamma_A \cdot \Delta H$ (Eq. (2.4)), between changes in area and changes in enthalpy, the excess isothermal lateral compressibility can be found from the excess heat capacity:

$$\begin{aligned} \Delta\kappa_T^A &= - \frac{1}{\langle A \rangle} \left(\frac{d}{d\Pi} \frac{\sum_i \Delta A_i \cdot e^{-H_i/RT}}{Z} \right)_T \\ &= \frac{\sum_i (\gamma_A \Delta H_i)^2 \cdot e^{-H_i/RT}}{\langle A \rangle RT \cdot Z} - \frac{1}{\langle A \rangle RT} \frac{\sum_i \gamma_A \Delta H_i \cdot e^{-H_i/RT}}{Z} \frac{\sum_j \gamma_A \Delta H_j \cdot e^{-H_j/RT}}{Z} \\ &= \gamma_A^2 \frac{\langle \Delta H^2 \rangle - \langle \Delta H \rangle^2}{\langle A \rangle RT} = \frac{\gamma_A^2 T}{\langle A \rangle} \Delta c_P. \end{aligned} \quad (\text{A.6})$$

This relation is “unique” to the lipid membrane, where the proportionality relation holds. Note that similar relations can be made using the proportionality relation between volume and enthalpy.

A.2 Relaxation Time

The relaxation behavior is of central importance for the present thesis. The following derivation is based on [18], and show that the single exponential relaxation behavior can be justified theoretically.

The distribution of states can be calculated from the Gibbs free energy. Assuming that the distribution of states are of Gaussian nature,

$$p(H - \langle H \rangle) = \frac{\exp(-G(H - \langle H \rangle)/RT)}{Z} = \frac{1}{\sigma\sqrt{2\pi}} \exp\left(-\frac{(H - \langle H \rangle)^2}{\sigma^2}\right). \quad (\text{A.7})$$

From this the Gibbs free energy can be written as,

$$G(H - \langle H \rangle) = -RT \ln(p(H - \langle H \rangle)) + \text{const.} \quad (\text{A.8})$$

The entropy can be written as a function of the Gibbs free energy and the enthalpy:

$$S(H) = \frac{-G(H) + H}{T} \Rightarrow \quad (\text{A.9})$$

$$S(H - \langle H \rangle) = \frac{H - \langle H \rangle}{T} - \frac{R(H - \langle H \rangle)^2}{2\sigma^2} - \frac{\text{const.}}{T} \quad (\text{A.10})$$

$$\approx \frac{R(H - \langle H \rangle)^2}{2\sigma^2}, \quad (\text{A.11})$$

where the approximation holds for small σ , which is equivalent to stating that the system is large. From this, the entropy takes the form of a harmonic potential, continuing this analogy the thermodynamical force driving the system back to equilibrium can be written as,

$$X(H - \langle H \rangle) = \left(\frac{\partial^2 S(H - \langle H \rangle)}{\partial(H - \langle H \rangle)^2} \right) (0) \cdot (H - \langle H \rangle) = \frac{R(H - \langle H \rangle)}{\sigma^2}. \quad (\text{A.12})$$

The flux back to equilibrium is,

$$\frac{d(H - \langle H \rangle)}{dt} = L \cdot X(H - \langle H \rangle) = -L \cdot \frac{R(H - \langle H \rangle)}{\sigma^2}. \quad (\text{A.13})$$

Eq. (A.13) is the rate equation taking the change in enthalpy back to equilibrium. Solving the rate equation the relaxation function of enthalpy can be written as,

$$H - \langle H \rangle = (H - \langle H \rangle)(0) \exp\left(-\frac{R \cdot L}{\sigma^2} t\right) \quad (\text{A.14})$$

$$\equiv (H - \langle H \rangle)(0) \exp\left(-\frac{t}{\tau}\right). \quad (\text{A.15})$$

Remembering Eq. (A.4),

$$c_P = \frac{d\langle H \rangle}{dT} = \dots = \frac{\langle H^2 \rangle - \langle H \rangle^2}{RT^2} = \frac{\sigma^2}{RT^2},$$

from this, the relaxation time can be written as,

$$\tau = \frac{T^2 c_p}{L}. \quad (\text{A.16})$$

This is a theoretical derivation of the proportionality relation between the relaxation time and the heat capacity. The only assumption in this derivation is the Gaussian nature of the distribution function and that the mean squared deviation of enthalpy is small.

Appendix B

Equation of Sound

The equation of sound will here be derived on the basis of fluid dynamics. The basic fluid dynamical equations needed for the present derivation are described in [Fluid Dynamics](#) (see appendix [B.1](#)).

Sound is a small amplitude oscillatory motion in a compressible fluid. Since the amplitude of the oscillations is small, only small perturbations will take place

$$p = p_0 + p', \quad \rho = \rho_0 + \rho'. \quad (\text{B.1})$$

The flow (velocity), generated by the small perturbations of the system will also be small. From this the equation of continuity Eq. [\(B.9\)](#) can be approximated to first order,

$$\frac{\partial \rho'}{\partial t} + \rho_0 \nabla \cdot \mathbf{v} = 0. \quad (\text{B.2})$$

Using that the velocity is small, Euler's equation Eq. [\(B.13\)](#) can in a similar manner be reduced to,

$$\frac{\partial \mathbf{v}}{\partial t} + \frac{1}{\rho} \nabla p = 0. \quad (\text{B.3})$$

This expression is valid when the velocity of the particles in the fluid generated by the sound perturbations are much smaller than the velocity of sound, $v \ll c$.

Utilizing the fact that a sound wave in a ideal fluid is adiabatic, one can relate the change in pressure p' to the change in density ρ' in the following manner,

$$p' = \left(\frac{\partial p}{\partial \rho} \right)_S \rho'. \quad (\text{B.4})$$

Inserting this into Eq. [\(B.2\)](#), one finds,

$$\frac{\partial p'}{\partial t} + \rho_0 \left(\frac{\partial p}{\partial \rho} \right)_S \nabla \cdot \mathbf{v} = 0. \quad (\text{B.5})$$

Eq. (B.3) and Eq. (B.5) are sufficient to completely describe a sound wave. A more convenient and standard form is achieved by introducing a velocity potential $\mathbf{v} \equiv \nabla\phi$, using this Eq. (B.3) takes the form,

$$p' = -\rho_0 \frac{\partial \phi}{\partial t}. \quad (\text{B.6})$$

Since the perturbations are small we approximate $p_o \approx p$ and $\rho_0 \approx \rho$. Using the definition of the velocity potential and Eq. (B.6), Eq. (B.5) can be formulated as following,

$$\frac{\partial^2 \phi}{\partial t^2} + c^2 \nabla^2 \phi = 0, \quad (\text{B.7})$$

where

$$c = \sqrt{\frac{\partial p}{\partial \rho}}_S = \frac{1}{\sqrt{\kappa_S \rho}}, \quad (\text{B.8})$$

is the velocity of sound. κ_S is the adiabatic compressibility. This is the general *equation of sound* or *wave equation*. This basic introduction to sound is base on [92].

B.1 Fluid Dynamics

In this section the fundamental equations of fluid dynamics for ideal fluids will be briefly described.

For any system where no chemical reaction or similar takes place, conservation of matter can be easily be converted into the *equation of continuity*,

$$\frac{\partial \rho}{\partial t} + \nabla \cdot (\rho \mathbf{v}) = 0, \quad (\text{B.9})$$

where ρ is the density and \mathbf{v} is the velocity of a given volume element. The equation of continuity states that any change in density is equal to the density moving in or out of the volume element in question.

Fluid dynamics is the study of motion in fluids. To achieve a net motion in any system a force have to be applied. Consider a volume element of a fluid, the force acting on this element is given by

$$\mathbf{F} = \int \rho \frac{d\mathbf{v}}{dt} dV = \oint p d\mathbf{f} = \int \nabla p dV. \quad (\text{B.10})$$

From this the following must hold,

$$\rho \frac{d\mathbf{v}}{dt} = \nabla p, \quad (\text{B.11})$$

where p is the pressure exerted onto the element by its surrounding and the integral is over the volume. The $d\mathbf{v}/dt$ denotes the change in velocity of a given volume element. The change in velocity can be decomposed into

$$d\mathbf{v} = dx \frac{\partial \mathbf{v}}{\partial x} + dy \frac{\partial \mathbf{v}}{\partial y} + dz \frac{\partial \mathbf{v}}{\partial z} + dt \frac{\partial \mathbf{v}}{\partial t} = dt \frac{\partial \mathbf{v}}{\partial t} + (\mathbf{r} \cdot \nabla) \mathbf{v}, \quad (\text{B.12})$$

where \mathbf{r} is the position vector. Dividing through with dt , Eq. (B.12) can be substituted into Eq. (B.11) giving *Euler's equation*,

$$\frac{\partial \mathbf{v}}{\partial t} + (\mathbf{v} \cdot \nabla) \mathbf{v} = -\frac{1}{\rho} \nabla p. \quad (\text{B.13})$$

Euler's equation is the equation of motion for an *adiabatic ideal* system. In the presented derivations dissipation of any kind have not been taken into account (ideal system). Further note that heat exchange between different volume elements of the fluid is not considered, making the system adiabatic.

The last fundamental equation in fluid dynamics is the *equation of entropy conservation* that states

$$\frac{\partial(\rho s)}{\partial t} + \nabla \cdot (\rho s \mathbf{v}) = 0, \quad (\text{B.14})$$

where s is the entropy of a given volume element. Similarly to the equation of continuity, this equation states that a change in entropy is equal to the entropy going in or out of the volume element [92].

Appendix C

Derivations

This section will contain the essential derivations used in the thesis, which have been omitted due to their length.

C.1 Latent Heat of Expansion

In the section on the [Adiabatic Pressure Perturbations](#) (section 3.1) the thermodynamical implications of an adiabatic low amplitude pressure perturbation is considered. From a thermodynamical point of view these changes in pressure and temperature couples to a change in the heat of the system,

$$dQ = c_P dT - L_P dP, \quad (\text{C.1})$$

where dQ is the change in the heat of the system, c_p is the heat capacity and L_p is the latent heat of expansion. The latent heat of expansion can be written as [68]

$$L_P = \left(\frac{dH}{dP} \right)_T - V. \quad (\text{C.2})$$

Using the fact that an infinitesimal change in enthalpy can be written as

$$dH = dU + PdV + VdP, \quad (\text{C.3})$$

Eq. (C.2) can be rewritten,

$$L_P = \left(\frac{dU}{dP} \right)_T + P \left(\frac{dV}{dP} \right)_T = \left(\left(\frac{dU}{dV} \right)_T + P \right) \left(\frac{dV}{dP} \right)_T. \quad (\text{C.4})$$

By rewriting the derivative of the energy,

$$\left(\frac{dU}{dV} \right)_T = T \left(\frac{dS}{dV} \right)_T - P \quad (\text{C.5})$$

$$= -T \left(\frac{d^2 F}{dT dV} \right) - P \quad (\text{C.6})$$

$$= T \left(\frac{dP}{dT} \right)_V - P, \quad (\text{C.7})$$

where $dF = -SdT - PdV$ and F is the Helmholtz free energy. From this Eq. (C.4) takes the form:

$$L_P = T \left(\frac{dP}{dT} \right)_V \left(\frac{dV}{dP} \right)_T \quad (\text{C.8})$$

$$= T \left(\frac{dS}{dV} \right)_T \left(\frac{dV}{dP} \right)_T \quad (\text{C.9})$$

$$= T \left(\frac{dS}{dP} \right)_T \quad (\text{C.10})$$

$$= T \left(\frac{d^2G}{dT dP} \right) = -T \left(\frac{dV}{dT} \right)_P \quad (\text{C.11})$$

$$= -TV\alpha_P, \quad (\text{C.12})$$

where G is the Gibbs free energy and α_P is the thermal expansion coefficient.

C.2 Real Part of the Phase Velocity

The lateral phase velocity is related to the adiabatic lateral compressibility through Eq. (2.13),

$$c^A = \frac{1}{\sqrt{\kappa_S^A \rho^A}}.$$

Both the lateral phase velocity and the adiabatic lateral compressibility are complex quantities,

$$\operatorname{Re}(c^A) + i\operatorname{Im}(c^A) = \frac{1}{\sqrt{\rho^A (\operatorname{Re}(\kappa^A) + i\operatorname{Im}(\kappa^A))}}. \quad (\text{C.13})$$

The goal of the thesis is to estimate the real part of the lateral phase velocity. For this the real part of the complex lateral phase velocity has to be isolated. This can be done as follows, from Eq. (C.13):

$$\operatorname{Re}(c^A)^2 - \operatorname{Im}(c^A)^2 + i2\operatorname{Re}(c^A)\operatorname{Im}(c^A) = \frac{1}{\rho^A} \frac{\operatorname{Re}(\kappa^A) - i\operatorname{Im}(\kappa^A)}{\operatorname{Re}(\kappa^A)^2 + \operatorname{Im}(\kappa^A)^2} \quad (\text{C.14})$$

Recognizing the real and the complex parts respectively,

$$\operatorname{Re}(c^A)^2 - \operatorname{Im}(c^A)^2 = \frac{1}{\rho^A} \frac{\operatorname{Re}(\kappa^A)}{\operatorname{Re}(\kappa^A)^2 + \operatorname{Im}(\kappa^A)^2}, \quad (\text{C.15})$$

$$2\operatorname{Re}(c^A)\operatorname{Im}(c^A) = -\frac{1}{\rho^A} \frac{\operatorname{Im}(\kappa^A)}{\operatorname{Re}(\kappa^A)^2 + \operatorname{Im}(\kappa^A)^2}. \quad (\text{C.16})$$

From the last expression the imaginary part of the lateral phase velocity can be isolated,

$$\operatorname{Im}(c^A) = -\frac{1}{\rho^A} \frac{1}{2\operatorname{Re}(c^A)} \frac{\operatorname{Im}(\kappa^A)}{\operatorname{Re}(\kappa^A)^2 + \operatorname{Im}(\kappa^A)^2}, \quad (\text{C.17})$$

which can be inserted into the square of the real part of the complex lateral phase velocity:

$$\operatorname{Re}(c^A)^2 = (\rho^A)^{-1} \left(\frac{\operatorname{Re}(\kappa^A) + \sqrt{\operatorname{Re}(\kappa^A)^2 + 4\operatorname{Im}(\kappa^A)^2}}{2(\operatorname{Re}(\kappa^A)^2 + \operatorname{Im}(\kappa^A)^2)} \right) \quad (\text{C.18})$$

The imaginary part of the lateral phase velocity can be found in a similar fashion by isolating the real part in Eq. (C.16).

Appendix D

Linear Response Theory

The relaxation behavior of a system can be studied by exploring how a system subject to perturbations relaxes back to a new equilibrium. This is ensured by the fluctuation-dissipation theorem that states, that the response of a system in equilibrium to a small perturbation is the same as the systems response to spontaneous fluctuations [90]. If the perturbation is sufficiently small it is often assumed that the rate equations that governs the relaxation can be well approximated by a linear function of the perturbation, often referred to as *linear perturbation theory* or *linear response theory* [67].

The basic linear rate equation is as follows:

$$\frac{d\Delta\alpha(t)}{dt} = -\frac{\Delta\alpha(t)}{\tau}, \quad \Delta\alpha(t) = \alpha(t) - \alpha_0, \quad (\text{D.1})$$

where τ is the relaxation time, α is the variable under consideration and α_0 is the variable value at equilibrium. The solution to Eq. (D.1) is

$$\Delta\alpha(t) = \Delta\alpha(0) \cdot \exp\left(-\frac{t}{\tau}\right), \quad (\text{D.2})$$

where $\Delta\alpha(0)$ is the initial extent of the applied perturbation. In Eq. (D.1) it is assumed the system has been moved out of equilibrium to $\Delta\alpha(0)$ in a instantaneous jump. Assuming instead a periodic perturbation of the system the linear rate equation has to be rewritten;

$$\frac{d\Delta\alpha(t)}{dt} = -\frac{\Delta\alpha(t) - \Delta\alpha_p(t)}{\tau}, \quad (\text{D.3})$$

where $\Delta\alpha_p(t)$ is the periodic perturbation. The periodic perturbation of interest, in this thesis, is of sinusoidal nature,

$$\Delta\alpha_p(t) = a_\alpha \exp(i\omega t), \quad (\text{D.4})$$

where ω is the angular frequency of the perturbation and a_α is the amplitude of the perturbation. Assuming the sinusoidal nature of the perturbation the general solution to Eq. (D.3) is

$$\Delta\alpha(t) = \frac{a_\alpha \exp(-t/\tau)}{\tau} \int_{-\infty}^t \exp(t'/\tau + i\omega t') dt'. \quad (\text{D.5})$$

Carrying out the integration,

$$\Delta\alpha(t) = \frac{\Delta\alpha_p(t)}{1 + i\omega\tau} = \frac{a_\alpha \exp(i(\omega t - \theta))}{(1 + (\omega\tau)^2)^{1/2}}, \quad (\text{D.6})$$

where

$$\tan(\theta) = \omega\tau. \quad (\text{D.7})$$

This means that there will be a phase lag between the perturbation and the response and a drastic lowering amplitude of the respond, when the system is perturbed faster then it can respond.

Note that linear response theory is based on the assumption of a linear response which has to be verified for a given application.

Appendix E

Simulations

This appendix section contains the supplementary information regarding the simulation effort of this thesis.

E.1 Detailed Balance of the Adiabatic Model

Detail Balance is defined as

$$p_a p(a \rightarrow b) = p_b p(b \rightarrow a) \quad (\text{E.1})$$

where p_a is the probability of being in the state a and $p(a \rightarrow b)$ is the transition probability for going from a to b and visa versa. A more convenient form of Eq. (E.1) is,

$$\frac{p_a}{p_b} = \frac{p(b \rightarrow a)}{p(a \rightarrow b)}. \quad (\text{E.2})$$

The probability of being in a given state is given by the free energy of that state

$$p_a = \frac{1}{Z} \exp\left(\frac{-G_a}{RT}\right), \quad (\text{E.3})$$

where Z is the partition sum.

For the adiabatic model:

$$p_a = p_{l,a} p_{r,a} = \frac{1}{Z} \exp\left(\frac{-G_{l,a}}{RT}\right) \exp\left(\frac{-G_{r,a}}{RT}\right) \quad (\text{E.4})$$

and

$$\frac{p_a}{p_b} = \exp\left(\frac{-\Delta G_l}{RT}\right) \exp\left(\frac{-\Delta G_r}{RT}\right), \quad (\text{E.5})$$

where $\Delta G = G_b - G_a$, the subscript r refer to the heat reservoir and l refer to the lipid membrane. From Eq. (4.27)

$$\frac{p(b \rightarrow a)}{p(a \rightarrow b)} = \frac{\frac{K}{K+1} \frac{K'}{K'+1}}{\frac{K^{-1}}{K^{-1}+1} \frac{K'^{-1}}{K'^{-1}+1}} \quad (\text{E.6})$$

$$= KK' = \exp\left(\frac{-\Delta G_l}{RT}\right) \exp\left(\frac{-\Delta G_r}{RT}\right), \quad (\text{E.7})$$

from the this the adiabatic model extension upholds detail balance.

E.2 Equilibration

The starting configuration of the system is, in simulations, either random or an estimate of a likely configuration. Independent of this, the system can not be considered to be in equilibrium from a start. By sampling before equilibrium has been achieved, there is no guarantee that the simulation estimations will have any resemblance with the actual system that is modeled. In general, the ergodic theorem and detailed balance only insures that equilibrium can be reach but not when. The equilibration time (Monte Carlo cycles) depends very much on the specific rejection algorithm. The general consensus for estimating when the system is equilibrated is to monitor when the mean of a given observable variable becomes constant. This often take place within a couple of correlation time scale (relaxation time) – illustrated in Fig. (E.1).

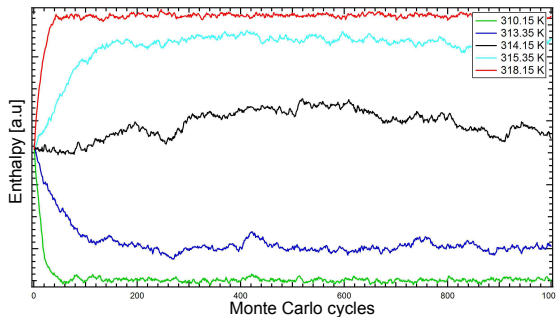


Figure E.1: Raw simulation data of the system mean enthalpy for five different temperatures, centered around $T = 314.15 K$.

It is clearly illustrated by Fig. (E.1) that the relaxation time in the simulations goes up quite drastically in the transition region, and extra care has to be taken to ensure equilibration in this region.

E.3 Finite Size Effects

The model system considered in the simulations of the present thesis, is one of the mono-layers in a lipid bilayer, which is infinite in extent in the plane. In a actual simulation the size of the simulated system is finite, which will introduce boundaries. Periodic boundary conditions have been implemented in all simulations to avoid boundary effects.

As mentioned in [Membrane Phase Transition](#) (section 2.1.3) the nature of the lipid melting transition is highly cooperative, but still finite in cooperativity. This means that the simulated system must be strictly bigger than the largest cooperative units in the simulation. Using the coupling between cooperative size and the heat capacity, the heat capacity can be used as a straightforward measure of the cooperative unit size. From Fig. (E.2) a system size above 64×64 lipid is sufficient to avoid finite size effects.

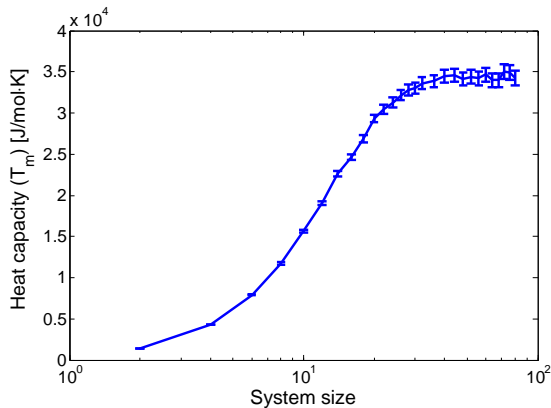


Figure E.2: Simulations of the excess heat capacity for systems of different sizes, at $T = 314.15\text{ K}$. The number of lipids in the system is system size squared.

E.4 Calculation of Errors

As with experiments Monte Carlo simulations are subject to errors: *statistical errors* and *systematic errors*.

Statistical errors arise from random fluctuations in the simulated system. Systematic errors are errors introduced by the procedure used to conduct the experiment or in the measuring method. In Monte Carlo simulations the systematic errors are in the equilibration, and inhered in a given model. The statistical nature of Monte Carlo simulations will inadvertently introduce statistical errors, these will be the focus of error estimation.

The simulations estimate of a mean value of a system variable is determined with an error. The standard measure of the error is the *standard deviation* given by

$$\sigma = \sqrt{\frac{1}{n_{independent} - 1} \sum (H_i - \langle H \rangle)^2} = \sqrt{\frac{1}{n - 1} (\langle H^2 \rangle - \langle H \rangle^2)} \quad (\text{E.8})$$

where n is the number of statistically independent measuring points. Here the enthalpy is used as an example of a system variable.

The general consensus is that the maximum number of statistical independent measuring points in a given simulation is,

$$n_{independent} = \frac{t_{max}}{2\tau^{MC}}, \quad (\text{E.9})$$

where t_{max} is the length of the simulation or the total number of simulated points after the system have equilibrated and τ^{MC} is the correlation time of the simulation. Usually sampling is done at intervals shorter than the correlation time, such that successive points are not uncorrelated. This can however be accounted for by the follow variation of standard deviation,

$$\sigma = \sqrt{\frac{1 + 2\tau^{MC}/\Delta t}{n - 1} (\langle H^2 \rangle - \langle H \rangle^2)} \quad (\text{E.10})$$

where Δt is the “time” distance between two points in succession. For large n Eq. (E.10) can be approximated to the following using that $n = t_{max}/\Delta t$,

$$\sigma = \sqrt{2\tau^{MC}/t_{max} (\langle H^2 \rangle - \langle H \rangle^2)}. \quad (\text{E.11})$$

Note that Eq. (E.11) is independent of Δt . which can be chosen freely and only the correlation time is need to estimate the errors [86].

Estimating the susceptibility and it statistical error is somewhat more involved. The susceptibility is the derivatives of system variables but can in many systems be derived from the fluctuations of the system variables (see appendix A.1). There exists a number of schemes which can be used to estimate the error of the susceptibilities, two of these will be described in the following: The Blocking method and the Jackknife method¹.

E.4.1 The Blocking Method

The simples and most general method of error estimation is the *Blocking method*. It is carried out by dividing the given data set up into block and

¹The Jackknife method is related to the well known Bootstrap method [86] which will not considered in this project due to complications in implementation.

separately calculating the variable of interest (e.g. the heat capacity). The associated error is then calculated using Eq. (E.8) where the values of interest calculated from the different blocks are the measuring point. This method have some limitations, the error estimation is very dependable on the number of blocks and the block size. Divide a given data set into a large number of small blocks the method will estimate small errors since the number of points is large but there might be a large error in the calculated value of interest by having small blocks [86].

E.4.2 The Jackknife Method

The *Jackknife method* is carried out as follows: Consider a data set of n strictly statistical independent data points, meaning as noted two or more correlation times τ^{MC} between each point. From these data points the variable of interest, c , is calculate, along with n additional estimates of the variable, which are carried out by removing first: The first point in the set and calculating the variable, c_1 , from the $n - 1$ points left, then the second point is removed² and the variable, c_2 , is calculated. This is continued throughout the complete set of independent data points. The error is then calculated from the $n + 1$ estimated variable values:

$$\sigma = \sqrt{\sum_{i=1}^n (c_i - c)^2}. \quad (\text{E.12})$$

The Jackknife method gives good estimates of the error and will for an infinite data set give the exact estimate. It is however quite inefficient computational wise for large data sets and other methods should be considered for very large data sets, such as *the bootstrap method* [86].

The Jackknife method will in this thesis be used to estimate the error of the simulated excess heat capacity and due to the strict demand for statistical independent data points, the error estimate of the system values (e.g. fluid fraction) will be done by Eq. (E.8).

E.5 Adoptive Algorithm

As approaching the phase transition the characteristic timescale of the simulation, as for the real system, is slowed down drastically. To insure sampling is only of statistical independent data points, (Eq. (E.9)), and to optimize simulation time an adaptive algorithm has been implemented in the simulations.

²The first point is now part of the set, so the sampling is still done over $n - 1$ points.

As seen in Fig. (4.4), the heat capacity, c_P , is strongly correlated with correlation time, τ^{MC} . From this the heat capacity can be used to estimate the correlation time. The simulations are mainly carried out as temperature sweeps, starting the simulation at a temperature below the transition a working its way up through the transition. If the temperature steps, ΔT , are sufficiently small, the heat capacity from the temperature step before can be used to estimate the correlation time for the present temperature.

$$\tau^{MC} = \max \left(1, \frac{2 \cdot c_P}{100} \right) \quad (\text{E.13})$$

Note that the correlation time has to be an integer. Given how the heat capacity spikes in the transition the temperature step size can be control by the heat capacity simply by its magnitude.

$$\Delta T = \min \left(1, \frac{5}{\sqrt{c_P}} \right) \quad (\text{E.14})$$

The total number of Monte Carlo cycles, n_{sample} , sampled over, given a certain statistical precision, and the number of Monte Carlo cycles needed for equilibration, $n_{equilibration}$, can likewise be estimate from the heat capacity:

$$n_{sample} = 14 \cdot c_P \quad (\text{E.15})$$

$$n_{equilibration} = 3 \cdot c_P \quad (\text{E.16})$$

Remembering that both values need to be integer.

Starting the simulation temperature sweeps it is essential that the first heat capacity is well estimated. Standard values used, for the starting temperature 312.15 K, are the following:

τ^{MC}	50
n_{sample}	10000
$n_{equilibration}$	1000